Thymic macrophages consist of two populations with distinct localization and origin

Tyng-An Zhou[1], Hsuan-Po Hsu[1], Yueh-Hua Tu[2,3], Hui-Kuei Cheng[1], Chih-Yu Lin[1], Nien-Jung Chen[1], Jin-Wu Tsai[4], Ellen A. Robey[5], Hsuan-Cheng Huang[2,6], Chia-Lin Hsu[1], and Ivan L. Dzhagalov[1*]

[1]Institute of Microbiology and Immunology, National Yang Ming Chiao Tung University, Taipei, Taiwan

[2]Bioinformatics Program, Taiwan International Graduate Program, Institute of Information Science, Academia Sinica, Taipei, Taiwan

[3]Graduate Institute of Biomedical Electronics and Bioinformatics, National Taiwan University, Taipei, Taiwan

[4]Brain Research Center, National Yang Ming Chiao Tung University, Taipei, Taiwan

[5]Division of Immunology and Pathogenesis, Department of Molecular and Cell Biology, University of California, Berkeley, CA, United States

[6]Institute of Biomedical Informatics, National Yang Ming Chiao Tung University, Taipei, Taiwan

*Correspondence to Ivan L. Dzhagalov: ivan.dzhagalov@nycu.edu.tw, ORCID: 0000-0001-9209-4582

Mailing Address: Ivan L. Dzhagalov, Institute of Microbiology and Immunology, National Yang Ming Chiao Tung University, #155, Sec. 2, LiNong Street, Beitou, Taipei City, 11221, TAIWAN

Abstract

Tissue-resident macrophages are essential to protect from pathogen invasion and maintain organ homeostasis. The ability of thymic macrophages to engulf apoptotic thymocytes is well appreciated, but little is known about their ontogeny, maintenance, and diversity. Here, we characterized the surface phenotype and transcriptional profile of these cells and defined their expression signature. Thymic macrophages were most closely related to spleen red pulp macrophages and Kupffer cells and shared the expression of the transcription factor SpiC with these cells. Single-cell RNA sequencing showed that the macrophages in the adult thymus are composed of two populations distinguished by the expression of *Timd4* and *Cx3cr1*. Remarkably, *Timd4*$^+$ cells were located in the cortex, while *Cx3cr1*$^+$ macrophages were restricted to the medulla and the cortico-medullary junction. Using shield chimeras, transplantation of embryonic thymuses, and genetic fate mapping, we found that the two populations have distinct origins. *Timd4*$^+$ thymic macrophages are of embryonic origin, while *Cx3cr1*$^+$ macrophages are derived from adult hematopoietic stem cells. Aging has a profound effect on the macrophages in the thymus. *Timd4*$^+$ cells underwent gradual attrition, while *Cx3cr1*$^+$ cells slowly accumulated with age and, in older mice, were the dominant macrophage population in the thymus. Altogether, our work defines the phenotype, origin, and diversity of thymic macrophages.

Introduction

Tissue-resident macrophages are present in every organ and maintain local homeostasis through diverse functions ranging from protection against pathogens to tissue repair (Wynn et al., 2013). To perform their roles efficiently, macrophages acquire specialized phenotypes depending on the tissue microenvironment, and as a consequence, multiple subtypes exist, frequently within the same organ. For example, the spleen harbors red pulp macrophages specialized in red blood cell phagocytosis, marginal zone macrophages and metallophilic macrophages that are the first defense against blood-borne pathogens, T cell zone macrophages that silently dispose of apoptotic immune cells, and tingible-body macrophages that engulf less fit B cells in the germinal center (Baratin et al., 2017) (A-Gonzalez & Castrillo, 2018; Bellomo et al., 2018). Thus, tissue-resident macrophages represent a fascinating developmental system that allows enormous plasticity.

The last decade has seen a paradigm shift in our understanding of the development of tissue-resident macrophages. Contrary to the long-held belief that all macrophages derive from circulating monocytes (van Furth & Cohn, 1968), multiple studies have shown that many of them are long-lived cells with an embryonic origin that can maintain themselves in the tissues (reviewed in (Ginhoux & Guilliams, 2016)). Three waves of distinct progenitors settle the tissues and contribute in various degrees to the resident macrophages in each organ. The first wave consists of the yolk sac (YS)-derived primitive macrophages that enter all tissues and establish the earliest macrophage populations (Perdiguero & Geissmann, 2015) (Mass et al., 2016). In all organs, except for the brain and, partially, the epidermis, primitive macrophages are

replaced by the next wave consisting of fetal monocytes (Ginhoux et al., 2010) (Hoeffel et al., 2012) (Hoeffel et al., 2015) (Goldmann et al., 2016). The third wave comes from hematopoietic stem cells (HSCs)-derived monocytes that contribute to various degrees to the macrophage pool in different tissues. For example, these cells contribute little to the microglia in the brain, Langerhans cells in the epidermis, and alveolar macrophages in the lungs but substantially to most other organs (Hashimoto et al., 2013) (Epelman et al., 2014) (Sheng et al., 2015) (Liu et al., 2019). Moreover, the kinetics and timing of HSC-derived monocyte infiltration vary in different parts of the body. For some macrophage populations, such as the arterial macrophages and subcapsular lymph node macrophages, monocytes replace embryonic macrophages soon after birth and self-maintain after that with little contribution from circulating cells (Ensan et al., 2015) (Mondor et al., 2019). Others, such as heart macrophages, osteoclasts, and pancreatic islets macrophages, are progressively replaced at a low rate (Epelman et al., 2014) (Molawi et al., 2014) (Heidt et al., 2014) (Calderon et al., 2015) (Jacome-Galarza et al., 2019) (Yahara et al., 2020). A third group, such as the macrophages in the dermis and most of the gut macrophages, are constantly replaced by blood monocytes with relatively fast kinetics (Tamoutounour et al., 2013) (Bain et al., 2014). These conclusions have been extended to many different macrophage populations such as Kupffer cells, liver capsular macrophages, red pulp macrophages, testicular macrophages, large and small peritoneal macrophages, and T zone macrophages in the lymph nodes (Baratin et al., 2017) (Hashimoto et al., 2013) (Epelman et al., 2014) (Liu et al., 2019) (Sierro et al., 2017) (Mossadegh-Keller et al., 2017) (Lokka et al., 2020) (Wang et al., 2021) (Bain et al., 2016).

97 The recent revitalization in macrophage research has yet to reach thymic
98 macrophages. Although their prodigious phagocytic ability is well appreciated
99 (Surh & Sprent, 1994), little is known about the origin, diversity, and
100 maintenance of these cells. This gap in our knowledge is, partly, due to the
101 lack of a consensus about the surface phenotype of thymic macrophages.
102 Various groups have used different markers to identify these cells, such as
103 F4/80 and Mac-3 (LAMP-2) (Surh & Sprent, 1994), or CD4 and CD11b (Esashi
104 et al., 2003), or Mac-2 (galectin 3), F4/80 and ED-1 (CD68) (Liu et al., 2013).
105 Most commonly, researchers employ F4/80 and CD11b (Guerri et al., 2013)
106 (Lopes et al., 2018) (Kim et al., 2010) (Tacke et al., 2015). However, none of
107 these markers is macrophage-specific: F4/80 is also expressed on
108 eosinophils and monocytes (Gautier et al., 2012) (Ingersoll et al., 2010), while
109 CD11b is present on most myeloid cells. The lack of a clear phenotypic
110 definition of thymic macrophages has translated into the absence of models
111 that target genes specifically in this population. For example, although
112 macrophages in various organs have been successfully targeted with *Lyz2*^{Cre},
113 *Csf1r*^{Cre}, or *Cx3cr1*^{Cre}, very few studies have used these models in the thymus
114 (Tacke et al., 2015) (Wang et al., 2019) (Chan et al., 2020).
115 Only a handful of studies have explored the origin of thymic macrophages.
116 Several reports have indicated that these cells could be derived from T cell
117 progenitors in the thymus based on an improved single cell in vitro culture and
118 in vivo transplantation experiments (Wada et al., 2008) (Bell & Bhandoola,
119 2008). However, these conclusions have been questioned based on fate-
120 mapping experiments using *Il7r*^{Cre} that found very limited contribution of
121 lymphoid progenitors to thymic macrophages in vivo in unperturbed mice

122 (Schlenner et al., 2010). Most recently, Tacke et al. used parabiosis to rule out
123 circulating monocytes as a major source of thymic macrophages (Tacke et al.,
124 2015). The same study also performed fate-mapping experiments to show
125 that most thymic macrophages descend from *Flt3*$^{+}$ HSC-derived progenitors.
126 However, the contribution of earlier waves of hematopoiesis has not been
127 explored.

128 Here, we aimed to bring our knowledge of thymic macrophages on par with
129 other tissue-resident macrophages. We started by clearly defining thymic
130 macrophages according to the guidelines set by the Immunological Genome
131 Consortium (IMMGEN) (Gautier et al., 2012) and characterized their surface
132 phenotype and transcriptional signature. Using single-cell RNA sequencing
133 (scRNA-Seq), we identified two populations of thymic macrophages with
134 distinct localization. We explored the origin of these cells through genetic fate
135 mapping, shield chimeras, and embryonic thymus transplantation and
136 documented that different waves of progenitors give rise to the two
137 populations of thymic macrophages. Altogether our work fills an important gap
138 in our understanding of resident thymic macrophages and provides the
139 framework for future functional characterization of these cells.

140

141 **Results:**

142 **CD64, F4/80, and MerTK identify the macrophages in the thymus**

143 To unambiguously and comprehensively identify macrophages in the
144 thymus, we evaluated several of the prototypical macrophage markers –
145 MerTK, CD64, and F4/80 (Gautier et al., 2012). A population that was stained
146 with all three markers (Figure 1A). As staining with MerTK and F4/80 was

147 relatively dim even when the brightest fluorochromes (e.g., PE) were used
148 and could not be resolved fully from the isotype control (Figure 1 – figure
149 supplement 1), we chose to use CD64 vs. forward scatter (FSC) as the first
150 step in our gating strategy (Figure 1B). Among $CD64^{+}FSC^{hi}$ cells,
151 $F4/80^{+}CD11b^{lo}$ macrophages could be distinguished from $F4/80^{lo}CD11b^{+}$
152 monocytes.

153 The $CD64^{+}F4/80^{+}MerTK^{+}CD11b^{lo}FSC^{hi}$ cells had typical macrophage
154 morphology with abundant cytoplasm (Figure 1C). These cells did not
155 express lineage markers characteristic of T cells (CD3ε), B cells (CD19),
156 eosinophils (Siglec F), NK cells (NK1.1), neutrophils (Gr1), or plasmacytoid
157 dendritic cells (Siglec H) (Figure 1D). However, they expressed phagocytic
158 receptors such as TIM4, CD51, and Axl (Figure 1E). Immunofluorescent
159 staining with CD64, MerTK, and TIM4 in the thymic cortex confirmed the
160 presence of large cells positive for all three macrophage markers (Figure 1 –
161 figure supplement 2).

162 Importantly, $MerTK^{+}$ cells could not be labeled by intravenously injected
163 CD45 antibody (Figure 1F), proving that they reside in the parenchyma of the
164 organs and not in the blood vessels. Based on the above data, we will refer to
165 $CD64^{+}F4/80^{+}MerTK^{+}CD11b^{lo}FSC^{hi}$ cells as thymic macrophages. The smaller
166 $CD64^{+}F4/80^{lo}CD11b^{+}FSC^{hi}$ population did not express MerTK but most of
167 them expressed Ly6C, and we classified them as thymic monocytes.

168 Thymic macrophages expressed CD11c, MHC2, and SIRPα making them
169 partially overlap with $CD11c^{+}MHC2^{+}$ classical dendritic cells (cDCs), thus
170 making problematic the unambiguous identification of thymic cDCs based only
171 on these two markers (Figure 1 – figure supplement 3). Proper identification of

172 cDC in the thymus requires the exclusion of macrophages based on CD64 or
173 MerTK staining. Otherwise, the cDCs, particularly the SIRPα^+ cDC2 subset,
174 would be contaminated with macrophages that account for ~25% of cDC2
175 (Figure 1 – figure supplement 4).

176 Thymic macrophages were ~0.1% of all the cells in the thymus of young
177 adult mice and numbered ~4x10^5 on average per mouse (Figure 1G). We did
178 not find statistically significant differences in their percentages between 4 and
179 11 weeks of age. Still, there was a significant decline in their numbers with
180 age, consistent with the beginning of thymic involution (Figure 1H).

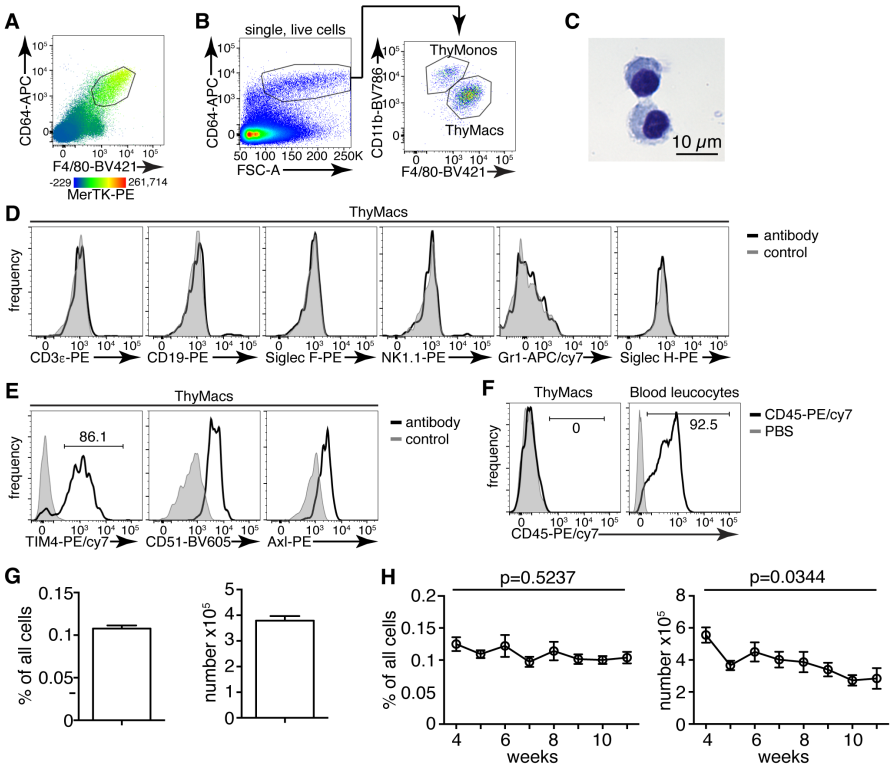

181

182 **Figure 1. Thymic macrophages (ThyMacs) can be identified by the**
183 **expression of CD64, MerTK, and F4/80. A** Flow cytometric analysis of
184 enzymatically digested thymus tissue with macrophage markers CD64,
185 MerTK, F4/80, and CD11b. **B** Gating strategy for identifying thymic
186 macrophages: CD64$^+$FSC^{hi} are first gated; the F4/80$^+$CD11b^{lo} cells among

187 them are the thymic macrophages (ThyMacs), while F4/80^{lo}CD11b^{+} are the
188 thymic monocytes (ThyMonos). **C** Pappenheim (Hemacolor Rapid staining
189 kit) staining of sorted ThyMacs. **D** Lack of expression of lineage markers
190 associated with other cell types on ThyMacs. **E** The expression on ThyMacs
191 of three receptors for phosphatidylserine that participate in the phagocytosis
192 of apoptotic cells. **F** Labeling of ThyMacs with intravenously injected anti-
193 CD45-PE antibody or PBS. The labeling of blood leucocytes is shown for
194 comparison. **G** Average numbers and percentages of ThyMacs in 4-11 weeks
195 old mice, n=82. **H** Comparison of the numbers and percentages of ThyMacs
196 in mice of different ages, n=82. All flow cytometry plots are representative of
197 at least 3 independent repeats. The numbers in the flow cytometry plots are
198 the percent of cells in the respective gates. Data in **G** and **H** represent
199 mean±SEM. Statistical significance in **H** was determined with one-way
200 ANOVA.

201

202 **Transcriptional signature of thymic macrophages**

203 To further understand the identity and functions of the thymic
204 macrophages, we analyzed the RNA sequencing data from the IMMGEN's
205 Open Source Mononuclear Phagocyte profiling. We first examined the
206 expression of the core signature macrophage genes (Gautier et al., 2012) and
207 found that they were enriched in thymic macrophages but not in *Sirpa*$^{+}$ or
208 *Xcr1*$^{+}$ thymic cDCs (Figure 2A). On the contrary, cDC core signature genes
209 were abundantly expressed in both thymic cDC subsets but not in thymic
210 macrophages. Thus, although thymic macrophages and cDCs share the

211 thymic microenvironment and expression of CD11c and MHC2, they have
212 distinct transcriptional profiles.
213 We then compared the gene expression profile of thymic macrophages to
214 that of other well-characterized macrophage populations from the IMMGEN
215 database. Because of the abundance of samples, we limited our comparison
216 to only nine types of tissue-resident macrophages under steady-state
217 conditions – splenic red pulp macrophages, Kupffer cells, broncho-alveolar
218 lavage macrophages, large peritoneal cavity macrophages, white adipose
219 tissue macrophages, aorta macrophages, central nervous system microglia,
220 and spinal cord microglia. Principal component analysis revealed that thymic
221 macrophages were most closely related to splenic red pulp macrophages and
222 Kupffer cells (Figure 2B).
223 To better identify the unique functions of thymic macrophages, we looked
224 for differentially expressed genes in these cells compared to other tissue-
225 resident macrophages. We set three criteria: 1) high expression in thymic
226 macrophages (>500); 2) >5-fold higher expression than the average value in
227 the nine populations of non-thymic macrophages; 3) expression in thymic
228 macrophages is higher than any non-thymic macrophage samples. A total of
229 44 genes met these criteria, and we consider them to constitute the
230 transcriptional signature of thymic macrophages (Figure 2C). These included
231 several degradation enzymes and their inhibitors (*Cst7*, *Mmp2*, *Mmp14*,
232 *Dnase1l3*, *Serpina3g*, *Acp5*), non-classical MHC molecules (*H2-M2*, *H2-Q6*,
233 *H2-Q7*), metabolic enzymes (*Chst2*, *Ass1*, *Kynu*, *Cp*, *Dgat2*, *Sorl1*, *Lap3*),
234 molecules involved in innate immunity (*Ifit2*, *Il18bp*, *Mefv*, *Lgals3bp*) and
235 extracellular signaling molecules and their receptors (*Pdgfa*, *Cxcl16*, *Il2rg*,

236 *Gpr157*). We also looked for transcription factors (TFs) highly expressed in
237 thymic macrophages and could potentially regulate critical gene networks in
238 these cells. A total of 25 TFs were highly expressed in thymic macrophages
239 (>250) and were at least 2-fold higher as compared to the non-thymic
240 macrophages (Table 1). Among them were several TFs involved in type I
241 interferon (IFN-I) signaling (*Stat1*, *Stat2*, *Irf7*, and *Irf8*) and lipid metabolism
242 (*Nr1h3*, *Pparg*, *Srebf1*, and *Rxra*) (Figure 2D). Notably, *Runx3*, which is
243 essential for the development and function of cytotoxic T lymphocytes
244 (Taniuchi et al., 2002), innate lymphoid cells (Ebihara et al., 2015), and
245 Langerhans cells (Fainaru et al., 2004), was highly expressed in thymic
246 macrophages. *Spic*, which has well-documented roles in the development of
247 red pulp macrophages in the spleen and bone marrow macrophages
248 (Kohyama et al., 2008) (Haldar et al., 2014), was also highly expressed in
249 thymic macrophages, further strengthening the argument for the similarity
250 between thymus, spleen, and liver macrophages. To confirm the expression
251 of *Spic* in thymic macrophages, we analyzed the thymus of $Spic^{GFP}$ mice
252 (Haldar et al., 2014). We found that all $Spic^{GFP+}$ cells were macrophages
253 (Figure 2 – figure supplement 1), making them the most specific thymic
254 macrophage reporter strain compared with $Lyz2^{GFP}$, MAFIA ($Csf1r^{GFP}$),
255 $Cd11c^{YFP}$, and $Cx3cr1^{GFP}$ mice (Figure 2 – figure supplement 2). However,
256 only ~80% of thymic macrophages were $Spic^{GFP+}$ suggesting heterogeneity
257 within the cells (Figure 2 – figure supplement 3).
258 Several dominant pathways emerged when we grouped the 500 most
259 highly expressed genes in thymic macrophages according to gene ontology
260 (GO) terms (Figure 2E). Notably, five of the ten most highly enriched GO

261 pathways concerned antigen presentation of both exogenous and
262 endogenous antigens. These data complement our flow cytometry findings of
263 expression of MHC2 and suggest that thymic macrophages could be potent
264 antigen-presenting cells and might play a role in negative selection or agonist
265 selection of thymocytes. Two other highly enriched GO pathways were
266 involved in lysosomal biogenesis and functions, highlighting the high capacity
267 of these cells to degrade phagocytosed material. Thus, our transcriptional
268 analysis has revealed that thymic macrophages are bona fide macrophages
269 that bear significant similarity to spleen and liver macrophages and are
270 specialized in lysosomal degradation of phagocytosed material and antigen
271 presentation.

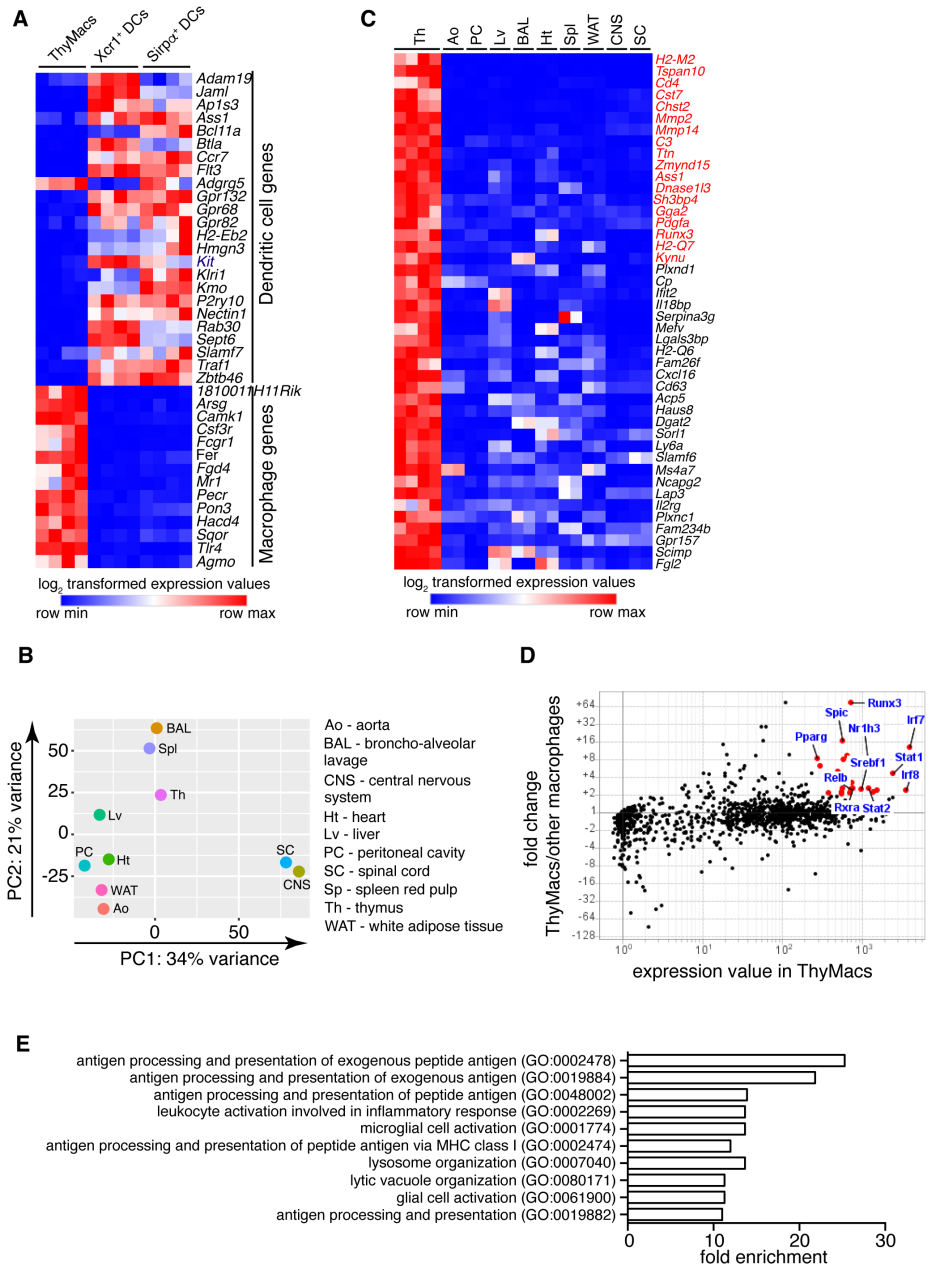

Figure 2. Transcriptional profile of thymic macrophages (ThyMacs). A Expression of cDC-specific genes (top) and macrophage-specific genes (bottom) in ThyMacs and two populations of thymic cDCs (ThyDCs) – *Xcr1*$^{+}$ ThyDCs and *Sirpa*$^{+}$ ThyDCs. **B** Principal components analysis of ThyMacs and nine other populations of tissue-resident macrophages in duplicates. **C** Highly expressed (>500) genes enriched (>5-fold) in ThyMacs (4 samples) compared to nine other tissue-resident macrophage populations (two samples each). The genes in red are >10-fold up-regulated in thymic macrophages. **D**

281 Comparison of the geometric mean expression of transcription factors in
282 thymic macrophages (4 samples) and the nine other macrophage populations
283 (2 samples each). Transcription factors with expression >250 and fold
284 change >2 are marked with red dots. **E** Top 10 GO pathways in ThyMacs
285 based on the 500 most highly expressed genes in these cells.
286

287 **Thymic macrophages can present antigens to T cells and clear**
288 **apoptotic cells**

289 Next, we investigated the biological functions of thymic macrophages. Our
290 findings that these cells express MHC2 and many other genes involved in
291 antigen presentations prompted us to test if they can efficiently activate T
292 cells. We pulsed sorted thymic macrophages with chicken ovalbumin (Ova)
293 and cultured them with naïve OT2 cells labeled with CFSE. The positive
294 control, thymic DCs, efficiently induced OT2 cell proliferation, while peritoneal
295 macrophages were very inefficient (Figure 3A and B), similar to other tissue-
296 resident macrophages (Baratin et al., 2017). Surprisingly, thymic macrophages
297 induced proliferation in a considerable proportion (~30%) of OT2 cells as
298 calculated by FlowJo's Proliferation Modeling module. Thus, thymic
299 macrophages are able antigen-presenting cells, although not as good as DCs.

300 To confirm the ability of thymic macrophages to clear apoptotic cells, we
301 did in vitro engulfment assay. Thymocytes were induced to undergo apoptosis
302 by Dexamethasone treatment and labeled with pHrodo Red dye. pHrodo Red
303 is weakly fluorescent at neutral pH, but its fluorescence increases significantly
304 at low pH, for example, in lysosomes. Thus, engulfed apoptotic cells can be
305 clearly identified by their strong red fluorescence. We incubated the pHrodo

306 Red-labeled apoptotic thymocytes for 2 hours with sorted thymic or peritoneal
307 cavity macrophages and detected the extent of efferocytosis by fluorescent
308 microscopy. Thymic macrophages were avid phagocytes, and we could
309 record many instances of efferocytosis at this time point (Figure 3C and D).
310 However, peritoneal macrophages were able to phagocytose even more
311 apoptotic cells.
312 To determine if thymic macrophages are the major phagocytes in the
313 thymus in vivo, we evaluated their participation in the phagocytosis of
314 apoptotic cells in the thymus by TUNEL staining. Most TUNEL$^+$ cells could be
315 found clearly inside or closely associated with MerTK$^+$ and TIM4$^+$ cells in the
316 thymus (Figure 3E and F). On average, ~85% of all TUNEL$^+$ cells were within
317 5 μm of MerTK$^+$ cells, confirming that thymic macrophages are the dominant
318 phagocytic population in the thymus (Figure 3G). The degree of co-
319 localization between TUNEL$^+$ cells and TIM4$^+$ cells was slightly lower, ~75%
320 on average, possibly reflecting the absence of TIM4 expression on a small
321 proportion of thymic macrophages (Figure 1E).
322

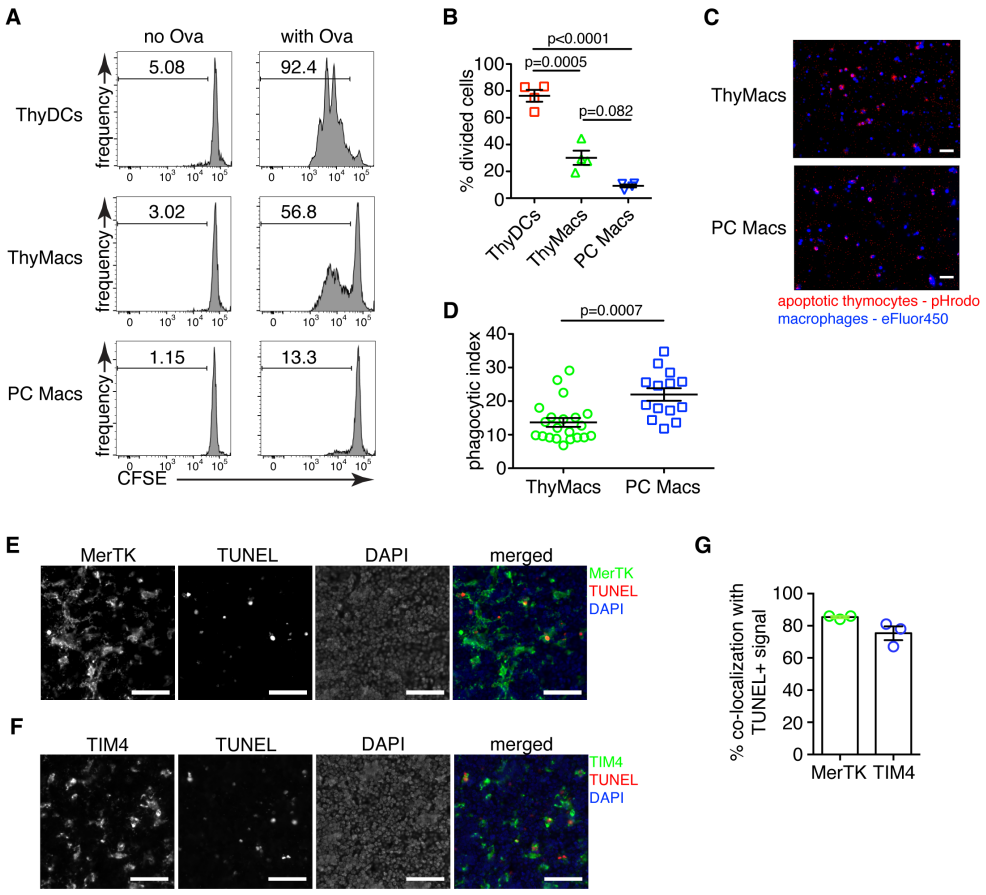

Figure 3. Thymic macrophages can present antigens to T cells and phagocytose apoptotic cells. A Naïve OT2 T cells were labeled with CFSE and cultured with purified thymic dendritic cells (ThyDCs), thymic macrophages (ThyMacs), or peritoneal cavity macrophages (PC Macs) in the presence or absence of chicken ovalbumin (Ova). Three days later, the CFSE dilution was assessed by flow cytometry. **B** Quantification of the cell division in naïve OT2 cells by using the Cell Proliferation module in FlowJo that calculates the percent of cells from the initial population that has undergone division. **C** Example immunofluorescent images of ThyMacs or PC Macs phagocytosis apoptotic thymocytes. The macrophages were labeled with eFluor 450, while the apoptotic thymocytes – with pHrodo Red. An intense red signal within the macrophages indicates phagocytosed thymocytes. **D** Quantification of the percentage of macrophages that have engulfed at least

337 one thymocyte (phagocytic index). **E** Example images showing co-localization
338 of TUNEL$^+$ apoptotic cells and MerTK$^+$ ThyMacs in thymic sections. **F**
339 Example images showing co-localization of TUNEL$^+$ apoptotic cells and TIM4$^+$
340 ThyMacs in thymic sections. Scale bars in **E** and **F** are 50 μm. **G** Frequencies
341 of the co-localization of TUNEL$^+$ signal with MerTK$^+$ and TIM4$^+$ cells. Flow
342 cytometry plots in **A** are representative of two independent experiments. All
343 immunofluorescent images are representative of at least 3 independent
344 repeats. Data in **B**, **D**, and **G** represent mean±SEM. Each symbol in **B** and **G**
345 is an individual mouse. Each symbol in **D** is a field of view.
346

347 **Expression of *Timd4* and *Cx3cr1 can distinguish* two populations of**
348 **thymic macrophages**

349 Our phenotypic characterization showed clear signs of heterogeneity within
350 thymic macrophages, including the presence of TIM4$^+$ and TIM4$^-$ cells (Figure
351 1E) and *Cx3cr1*$^{GFP+}$ and *Cx3cr1*$^{GFP-}$ cells (Figure 2 – figure supplement). To
352 determine the degree of thymic macrophage heterogeneity, we performed
353 single-cell RNA sequencing (scRNA-Seq) of sorted *Csf1r*$^{GFP+}$ and *Cd11c*$^{YFP+}$
354 thymic cells. *Csf1r* is required for the survival of most macrophages and is
355 considered their definitive marker (Witmer-Pack et al., 1993) (Sasmono et al.,
356 2003), while *Cd11c*^{YFP} is expressed in many myeloid cells, including
357 macrophages (Hume, 2011). Both reporters identified an overlapping set of
358 cells (Figure 4 – figure supplement 1). At least 7 clusters could be identified
359 and assigned to different cell types by specific marker expression (Figure 4A
360 and B), including macrophages, B cells, pDCs, contaminating thymocytes,
361 and multiple cDC clusters. Two clusters expressed the

362 macrophage/monocytes-specific transcription factor *Mafb* and high levels of
363 *Fcgr1* (CD64), *Mertk*, and *Adgre1* (F4/80), indicating that they are
364 macrophages (Figure 4 – figure supplement 2). An additional cluster
365 expressed *Mafb* together with *Fcgr1* and *Adgre1* but not *Mertk*, fitting the
366 description of monocytes. There was no expression of *Mafb* outside these
367 three clusters confirming that our flow cytometry gating had identified all
368 macrophages in the thymus. Once we zoomed onto *Mafb*-expressing cells,
369 we could distinguish three separate populations: 1) monocytes that expressed
370 high levels of *Ly6c2* and *Itgam* (CD11b) but did not express *Mertk*; 2) *Timd4*$^{+}$
371 (encoding TIM4) macrophages that also expressed high levels of *Spic* and
372 *Slc40a1*, but low levels of *Cx3cr1*; 3) *Cx3cr1*$^{+}$ macrophages that expressed
373 low levels of *Timd4*, *Spic*, and *Slc40a1* (Figure 4C and D). Both
374 macrophages and monocytes expressed *Fcgr1* (CD64). Thus, these data
375 indicate that thymic macrophages consist of two populations with distinct
376 expression profiles.
377 We confirmed the results from scRNA-Seq by flow cytometry. We could
378 identify discrete TIM4^{+}*Cx3cr1*$^{GFP-}$ and TIM4^{-}*Cx3cr1*$^{GFP+}$ macrophages (Figure
379 4E). There was even a TIM4^{+}*Cx3cr1*$^{GFP+}$ intermediate population that could
380 not be distinguished in the scRNA-Seq dataset, likely because of the lack of
381 statistical power. To determine the localization of the two distinct macrophage
382 populations, we stained thymic sections from *Cx3cr1*^{GFP} mice with an antibody
383 to MerTK. The *Cx3cr1*$^{GFP-}$ MerTK^{+} cells correspond to *Timd4*$^{+}$ macrophages,
384 while the *Cx3cr1*$^{GFP+}$MerTK^{+} cells would be the *Cx3cr1*$^{GFP+}$ macrophages.
385 Strikingly, the two macrophage populations showed distinct localization in
386 young mice. *Timd4*$^{+}$ macrophages were located in the cortex, while the

387 *Cx3cr1*$^{GFP+}$ macrophages resided in the medulla and the cortico-medullary
388 junction (Figure 4F). The result was confirmed with direct staining for TIM4
389 that showed intense signal in the cortex, particularly in the deep cortex, and
390 absence of staining in the medulla (Figure 4 figure supplement 3). However,
391 the medulla still featured many CD64^{+} macrophages.
392 To better understand the differences between the two populations of thymic
393 macrophages, we looked for differentially expressed genes. We included the
394 thymic monocytes in the comparison, as these cells clustered the closest to
395 macrophages. *Timd4*$^{+}$ macrophages expressed the highest levels of the
396 transcription factors *Spic*, *Maf*, and *Nr1h3*; the receptors for apoptotic cells
397 *Axl*, *Mertk*, and *Timd4*; and many Slc transporters such as *Slc40a1*, *Slc1a3*,
398 *Slco2b1*, *Slc11a1*, and *Slc7a7* (Figure 4G and Table 2). *Cx3cr1*$^{+}$
399 macrophages expressed high levels of the transcription factor *Runx3*; a
400 distinct set of phosphatidylserine receptors such as *Stab1*, *Anxa5*, and *Anxa3*;
401 many degradative enzymes such as *Mmp2*, *Mmp14*, *Dnase1l3*, *Acp5*, *Lyz2*,
402 *Ctsz*, *Ctss*, *Ctsd*, *Ctsl*; cytokines such as *Pdgfa*, *Cxcl16*, and *Ccl12*; and
403 molecules involved in MHC1 antigen presentation such as *B2m*, *H2-M2*, *H2-*
404 *K1*, *H2-Q7*. Thymic monocytes were characterized by differential expression
405 of the typical monocyte genes *Ly6c2*, *Ccr2*, and *S100a4*, and genes involved
406 in MHC2 antigen presentation such as *Ciita*, *H2-DMb1*, *H2-Ab1*, and *Cd74*.

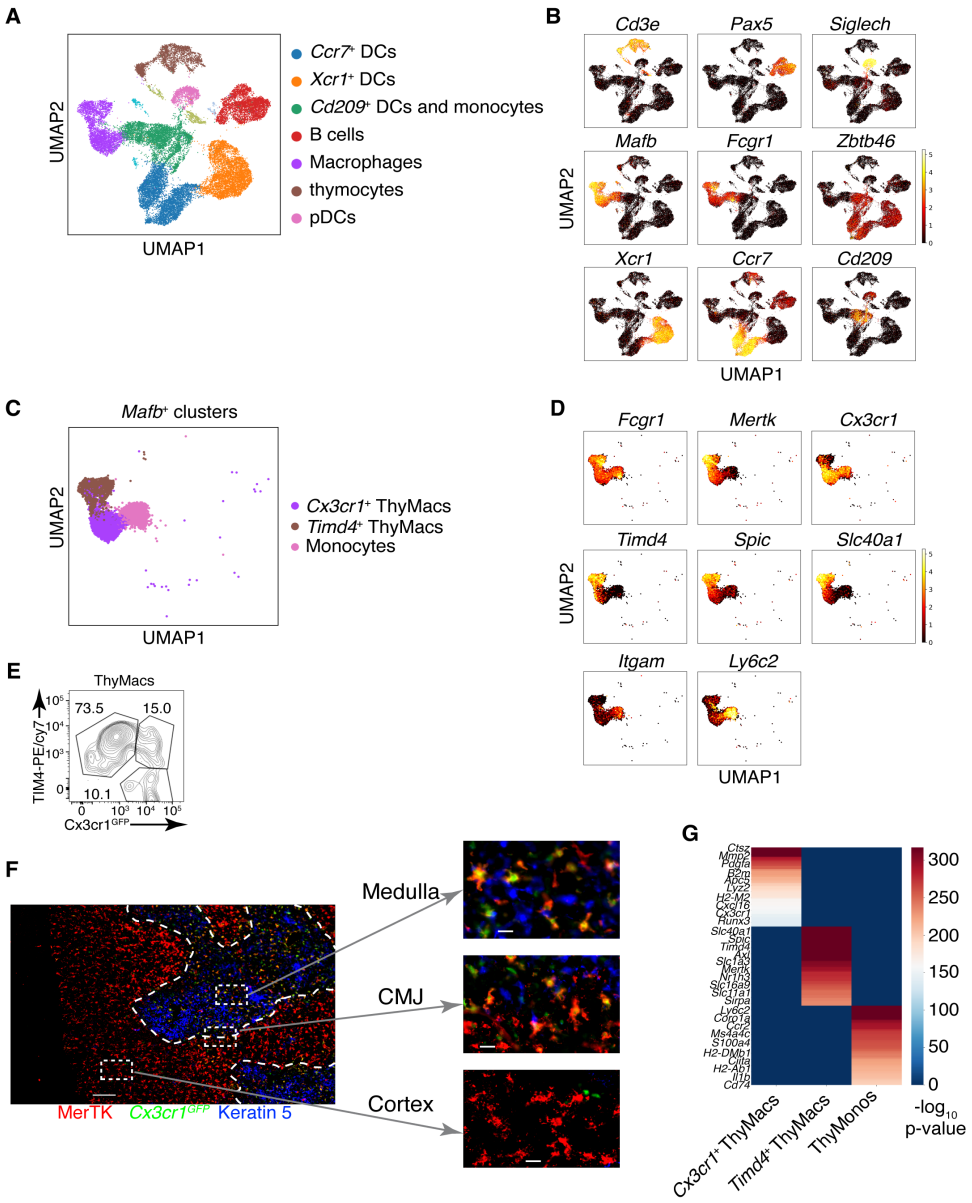

Figure 4: **Two populations of macrophages with distinct localization exist in the thymus. A** Identification of the clusters from the scRNA-Seq data based on lineage-specific markers. **B** Expression of lineage-specific markers in different clusters. **C** UMAP clusters from **A** with high expression of the transcription factor *Mafb* fall into three groups: monocytes, *Timd4*$^{+}$ macrophages, and *Cx3cr1*$^{+}$ macrophages. **D** Expression of the indicated genes in the three *Mafb*-positive clusters. **E** A flow cytometry plot of *Cx3cr1*^{GFP} and TIM4 expression in ThyMacs. The plot is representative of >10 individual experiments. The numbers inside the plot are the percentages of the cell

417 populations in the respective gates. **F** Immunofluorescent staining of the
418 thymus of *Cx3cr1*^{GFP} mouse stained with MerTK (a marker for all
419 macrophages) and Keratin 5 (a marker for medulla). The scale bar is 150 μm.
420 Areas in the cortex, medulla, and the cortico-medullary junction (CMJ)
421 represented by the dashed boxes are enlarged to the right to show the co-
422 localization of *Cx3cr11*^{GFP} and MerTK signal in CMJ and medulla, but not in
423 the cortex. The scale bars in the images to the right are 20 μm. The images
424 are representative of three individual mice. **G** Differentially expressed genes
425 among *Timd4*$^{+}$ thymic macrophages, *Cx3cr1*$^{+}$ thymic macrophages, and
426 thymic monocytes. The negative $\log_{10}$ p-values for the genes expressed in
427 each cluster were calculated as described in the Materials and Methods, and
428 the top 50 differentially expressed genes were plotted in the figure. Ten of
429 these genes are listed on the left.
430

431 **Yolk-sac progenitors contribute to embryonic thymic macrophages**

432 The ontogeny of thymic macrophages has been examined by only one
433 study since the realization that many tissue-resident macrophages are
434 descendants of embryonic progenitors (Tacke et al., 2015). Based on *Flt3*^{Cre}
435 fate-mapping, the authors concluded that most adult thymic macrophages
436 derive from HSCs. To determine if yolk-sac (YS) progenitors contribute to
437 embryonic thymic macrophages, we used *Cx3cr1*^{CreER} fate mapping (Yona et
438 al., 2013). Injection of 4-OHT at E9.5 in *ROSA26*$^{LSL\text{-}GFP}$ mouse mated with a
439 *Cx3cr1*^{CreER} male permanently tags YS progenitors and their descendants
440 with GFP (Figure 5A). Indeed, E19.5 microglia that are exclusively derived
441 from YS progenitors were labeled to a high degree (Figure 5B). After adjusting

442 for incomplete labeling based on the microglia, we found that at E15.5 >50%
443 of thymic macrophages were fate mapped, i. e. from YS origin (Figure 5C).
444 However, GFP$^+$ thymic macrophages decreased to just ~11% at E19.5,
445 suggesting that YS progenitors establish the embryonic thymic macrophage
446 pool but are quickly replaced by subsequent wave(s) of macrophages.
447

448 **Differential contribution of adult bone marrow-derived monocytes to**
449 **the two thymic macrophage populations**

450 To investigate the possibility that thymic macrophages arise from adult
451 bone marrow-derived monocytes, we devised two complementary
452 experiments. First, we evaluated the contribution of circulating adult
453 monocytes to thymic macrophages without the confounding effect of radiation
454 damage on the thymus. We created shield chimeras by subjecting CD45.2
455 mice to a lethal dose of irradiation while protecting their upper body and the
456 thymus with a 5 cm lead shield, followed by reconstitution with CD45.1 bone
457 marrow (Figure 5D). We analyzed *Timd4*$^+$ and *Cx3cr1*$^+$ thymic macrophages
458 separately after 6 weeks because we suspected they might have different
459 origins. As CX3CR1 protein expression was low on thymic macrophages
460 (Figure 5B), we defined the *Cx3cr1*$^+$*Timd4*$^-$ population as TIM4$^-$. The donor-
461 derived monocytes in the blood were, on average, 57%, but less than 2% of
462 TIM4$^+$ thymic macrophages were CD45.1$^+$ (Figure 5E and F), suggesting very
463 limited contribution of adult circulating monocytes to the TIM4$^+$ macrophage
464 pool. The percentage of HSC-derived TIM4$^-$ macrophages (on average 23%)
465 was intermediate between the monocytes and TIM4$^+$ macrophages, pointing
466 out that a sizeable part of TIM4$^-$ cells was derived from adult HSCs.

467 We also transplanted E15.5 thymuses from *Spic*$^{GFP+}$ CD45.2 embryos
468 under the kidney capsule of adult CD45.1 mice and analyzed them six weeks
469 later (Figure 5G). By that time, >99% of thymocytes in the transplanted
470 thymus were derived from CD45.1^{+} host HSCs, indicating successful
471 replacement by HSC-derived progenitors (Figure 5 – figure supplement 1).
472 TIM4^{-} thymic macrophages were derived entirely from host HSCs, just like
473 thymocytes. In contrast, most TIM4^{+} cells (on average 70%) were donor-
474 derived (Figure 5H and I). Moreover, only CD45.2^{+} TIM4^{+} macrophages
475 expressed *Spic*^{GFP} (Figure 5 – figure supplement 2). As expected, thymic
476 macrophages in the endogenous thymus were all CD45.1^{+}. The results from
477 our transplantation experiments show that the progenitors of most TIM4^{+}
478 thymic macrophages are of embryonic origin, while TIM4^{-} cells are derived
479 from adult monocytes. Altogether our results suggest that the two populations
480 of thymic macrophages have different origins. TIM4^{+} cells are derived from
481 embryonic precursors and can survive long-term without much contribution
482 from adult HSC and monocytes. In contrast, TIM4^{-} thymic macrophages rely
483 mostly on adult HSCs for their generation and replacement.

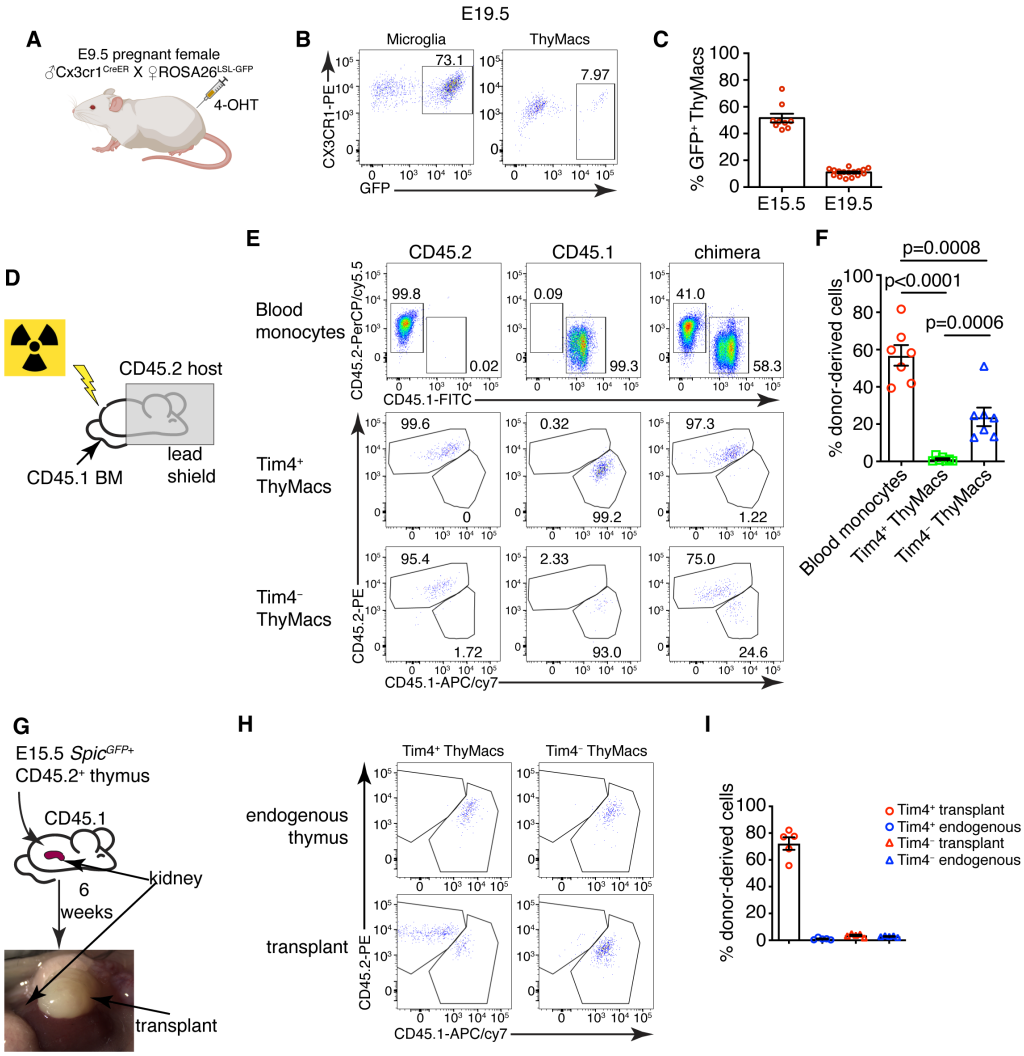

484

485 **Figure 5. Yolk sac (YS), non-YS-derived embryonic progenitors, and**

486 **adult hematopoietic stem cells sequentially contribute to the thymic**

487 **macrophage pool. A** Scheme of the YS-progenitor labeling experiments.

488 E9.5 pregnant *ROSA26*$^{LSL\text{-}GFP}$ mice mated with *Cx3cr1*^{CreER} males were

489 injected with 4-hydroxytamoxifen (4-OHT) and sacrificed at E15.5 or E19.5. **B**

490 Representative flow cytometry plots of the *Cx3cr1*^{GFP} expression in microglia

491 (CD45^{+}CD11b^{+} cells in the brain) and ThyMacs of the pups at E19.5. **C**

492 Frequencies of GFP^{+} ThyMacs at E15.5 and E19.5 adjusted to the degree of

493 labeling of microglia. **D** Scheme of the shield chimera experiments. Congenic

494 CD45.2 mice were lethally irradiated with their upper body protected by a 5

495 cm thick lead shield and then injected with CD45.1^{+} bone marrow. **E**

496 Representative flow cytometric analysis of CD115^{+}CD11b^{+} blood monocytes,
497 TIM4^{+} and TIM4^{-} thymic macrophages for donor-derived (CD45.1^{+}) and host-
498 derived (CD45.2^{+}) cells. Non-chimeric CD45.1 and CD45.2 samples serve as
499 controls for the gating. **F** Frequencies of donor-derived blood monocytes,
500 TIM4^{+} and TIM4^{-} ThyMacs. **G** Scheme of the thymus transplantation
501 experiments. Embryonic thymuses from E15.5 *Spic*$^{GFP+}$ CD45.2^{+} mice were
502 transplanted under the kidney capsule of CD45.1^{+} mice and analyzed six
503 weeks later. **H** Representative flow cytometry plots of donor (CD45.2^{+}) vs.
504 host (CD45.1^{+}) derived TIM4^{+} and TIM4^{-} ThyMacs in the transplanted thymus.
505 The host thymus (endogenous thymus) serves as a negative control. I
506 Frequencies of CD45.2^{+} (donor-derived) cells among TIM4^{+} and TIM4^{-}
507 ThyMacs in the transplanted and endogenous thymuses of the mice. Data in
508 **C**, **F**, and **I** are mean±SEM with two litters, seven, and five mice per group,
509 respectively. The numbers in the flow cytometry plots are the percent of cells
510 in the respective gates. Each symbol in the graphs is an individual mouse or
511 embryo.
512

513 **Thymic macrophages can proliferate in situ**

514 TIM4^{+} macrophages can persist for many weeks in the thymus without
515 constant replacement from blood monocytes, suggesting they can divide in
516 situ. Staining for the proliferation marker Ki67 revealed that ~4% of all thymic
517 macrophages expressed this marker compared to an isotype control (Figure
518 6A and B). To prove that thymic macrophages are proliferative, we tested the
519 incorporation of the nucleotide analog 5-Ethynyl-2'-deoxyuridine (EdU).
520 Short-term EdU labeling experiments unexpectedly revealed that thymic

521 macrophages become EdU$^+$ with faster kinetics than thymocytes (Figure 6 –
522 figure supplement 1). The most likely explanation for this puzzling result is
523 that some of the thymic macrophages have engulfed apoptotic thymocytes
524 that have recently divided and incorporated EdU. Thus, EdU could have
525 accumulated in these macrophages through phagocytosis, not cell division.
526 To circumvent this caveat, we designed a pulse-chase experiment (Figure
527 6C). Mice were injected daily with EdU for 21 days so that all cells that
528 proliferated in that period would incorporate the label. Most thymocytes and
529 thymic macrophages became EdU$^+$ at d. 21 (Figure 6D). After 21 more days
530 of "chase period", only ~0.2% of thymocytes had retained the EdU label,
531 consistent with the existence of a tiny population of long-term resident
532 thymocytes consisting mainly of regulatory T cells and NKT cells[54] (Figure
533 6D and E). However, ~5% of the thymic macrophages were EdU$^+$, suggesting
534 they divided during the labeling period. We also sorted thymic macrophages
535 and subjected them to cell cycle analysis. Although almost all thymic
536 macrophages were in G0/G1 phase, a small population of ~3% was in the
537 G2/M phase of the cell cycle (Figure 6F and G). Surprisingly, most *Mki67*$^+$
538 thymic macrophages belonged to the *Cx3cr1*$^+$ subset, and only a few of the
539 *Timd4*$^+$ cells were positive (Figure 6H). We confirmed this result from the
540 scRNA-Seq analysis experimentally. The expression of Ki-67 was significantly
541 higher in TIM4$^-$ than in TIM4$^+$ thymic macrophages (Fig. 6G), suggesting that
542 the former is the more proliferative subset. Collectively, four independent
543 approaches documented that a small proportion (3-5%) of thymic
544 macrophages are actively dividing under homeostatic conditions within the

545 thymus. The majority of the dividing cells were from the adult HSC-derived

546 *Cx3cr1*⁺ subset. *Timd4*⁺ macrophages were primarily quiescent.

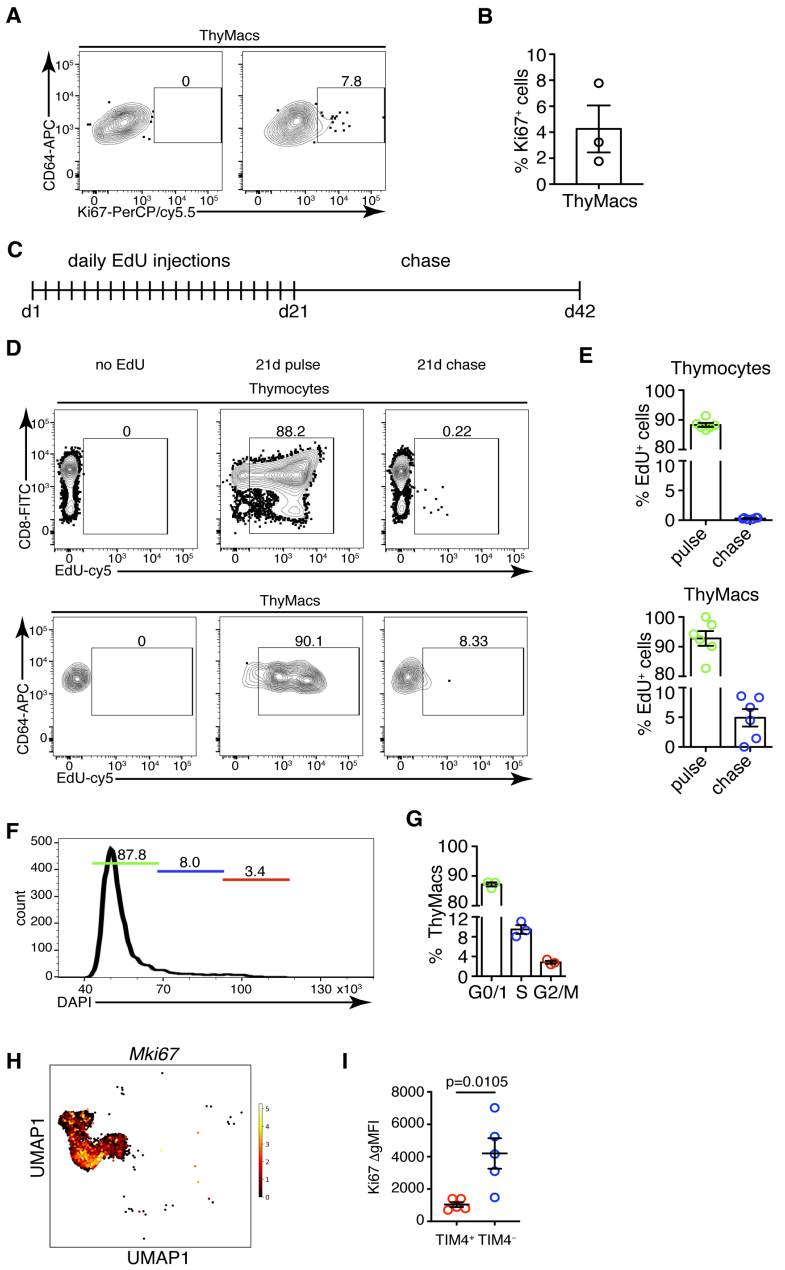

547

548 **Figure 6. Thymic macrophages exhibit a low degree of proliferation.**

549 **A** Example flow cytometry plots of Ki67 staining of thymic macrophages

550 (ThyMacs). **B** Frequency of Ki67⁺ thymic macrophages. **C** Scheme of EdU

551 pulse/chase experiment: mice were injected daily with 1 mg EdU i.p for 21

552 days and rested for 21 more days. **D** Example flow cytometry plots of EdU

553 staining of thymocytes (upper row) and ThyMacs (lower row). **E** Frequencies

554 of EdU$^+$ cells among thymocytes (top graph) and ThyMacs (bottom graph). **F**
555 Example flow cytometry plot of cell cycle analysis of FACS sorted ThyMacs. **G**
556 Frequencies of ThyMacs in different stages of the cell cycle. **H** UMAP plot of
557 *Mki67* expression in *Mafb*-positive clusters from the scRNA-Seq data
558 described in Figure 4. **I** Comparison of Ki67 protein expression in TIM4$^+$ and
559 TIM4$^-$ thymic macrophages. The expression is measured as the difference of
560 the geometric mean fluorescent intensities of the Ki67 antibody staining and
561 isotype control (ΔgMFI). The numbers in the flow cytometry plots are the
562 percent of cells in the respective gates. Data are mean±SEM from three mice
563 (**B** and **G**) or 5 mice (**I**), or 6-7 individual mice (**E**). Each dot is an individual
564 mouse. Statistical significance in (**I**) was determined by unpaired Student's t-
565 test.
566

567 ***Cx3cr1*$^+$ cells give rise to *Timd4*$^+$ cells during embryonic development**

568 To determine if the two populations of thymic macrophages are related, we
569 first analyzed the kinetics of their appearance during embryonic development.
570 At the earliest time point (E14.5), all thymic macrophages were *Cx3cr1*$^+$, and
571 only ~20% were also TIM4$^+$ (Figure 7A and B). The proportion of TIM4$^+$ cells
572 increased at E17.5, and TIM4$^+$*Cx3cr1*$^-$ cells started to appear. In the neonatal
573 period, almost all macrophages were TIM4$^+$, and very few remained TIM4$^-$.
574 The proportion of TIM4$^-$ cells increased in 6 weeks old mice, but TIM4$^+$
575 macrophages remained the dominant population. These kinetics (Figure 7C)
576 are consistent with *Timd4*$^+$ macrophages developing from *Cx3cr1*$^+$ cells
577 before birth. Another plausible scenario is that distinct progenitors give rise to
578 different thymic macrophage populations (e.g., YS-progenitors give rise to

579 *Cx3cr1*$^{+}$*Timd4*$^{-}$ and HSC-derived progenitors develop into *Timd4*$^{+}$
580 macrophages). To test the latter hypothesis, we revisited the fate mapping of
581 YS progenitors (Figure 5A). Although a larger part (~60% at E15.5) of fate-
582 mapped cells were *Cx3cr1*$^{+}$TIM4^{-} cells (Figure 7D), a substantial proportion
583 (~40% at E15.5) of fate-mapped TIM4^{+} macrophages could clearly be
584 identified at both E15.5 and E19.5, suggesting that YS progenitors can give
585 rise to both *Cx3cr1*$^{+}$ and *Timd4*$^{+}$ cells. Thus, the simplest explanation for our
586 findings is that *Timd4*$^{+}$ cells develop from *Cx3cr1*$^{+}$ cells during embryonic
587 development. This transition is complete in the first week after birth as there
588 were essentially no *Cx3cr1*$^{+}$TIM4^{-} thymic macrophages remaining at d.7
589 (Figure 7A and B). To formally demonstrate that *Cx3cr1*$^{+}$ macrophages can
590 give rise to *Timd4*$^{+}$ cells during embryonic development, we injected 4-OHT in
591 E15.5 pregnant females carrying *Cx3cr1*^{CreER} X *ROSA26*$^{LSL\text{-}GFP}$ fetuses (Fig.
592 7E). At this time almost all thymic macrophages are *Cx3cr1*$^{+}$ (Fig. 7A). Just
593 before birth, at E19.5, we could identify a sizeable population of
594 TIM4^{+}CX3CR1^{-} among fate-mapped cells, suggesting that they originate from
595 *Cx3cr1*$^{+}$ progenitors (Fig. 7F and G).

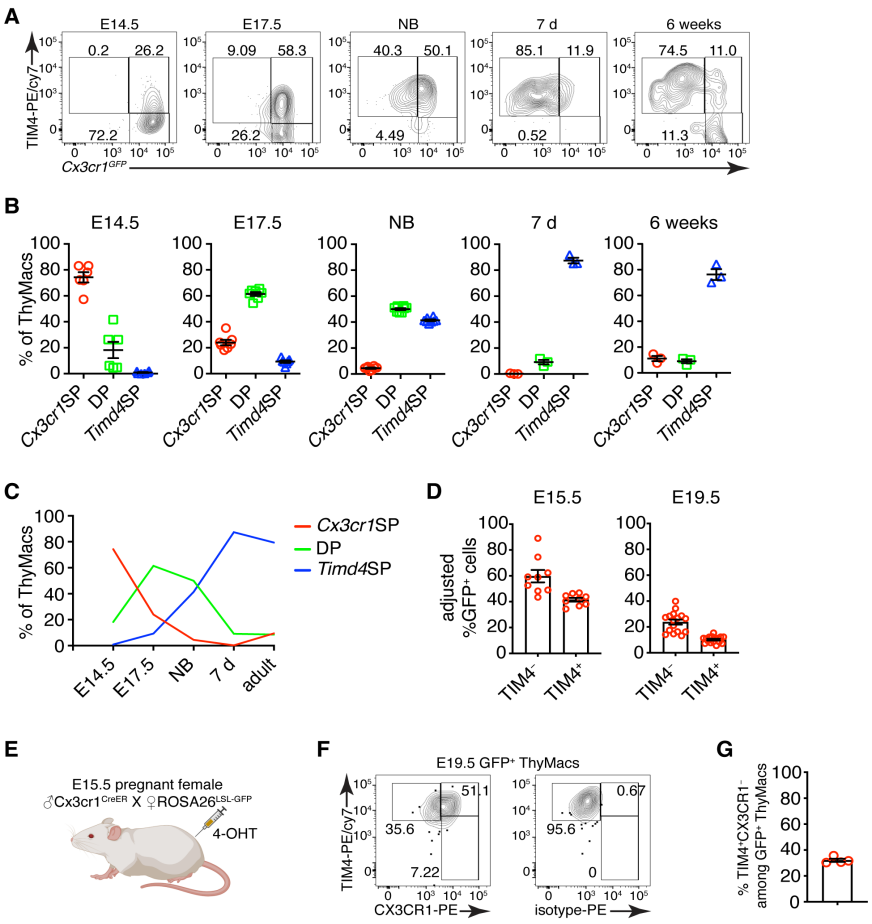

596

597 **Figure 7. *Timd4*⁺ thymic macrophages are derived from *Cx3cr1*⁺ cells**

598 **during embryonic development. A** Example flow cytometry plots for the

599 expression of *Cx3cr1*^{GFP} and TIM4 on thymic macrophages at different times

600 during embryonic development (E14.5, E17.5), immediately after birth, at 7

601 days, and 6 weeks of age. **B** Frequencies of *Timd4*⁺*Cx3cr1*⁻ (*Timd4* single-

602 positive or *Timd4*SP), *Timd4*⁺*Cx3cr1*⁺(double-positive or DP), and

603 *Cx3cr1*⁺*Timd4*⁻ (*Cx3cr1* single-positive or *Cx3cr1*SP) thymic macrophages at

604 the indicated time points. **C** Kinetics of the changes in different subpopulations

605 of thymic macrophages from E14.5 to 6 weeks. **D** Frequencies at E15.5 and

606 E19.5 of GFP-labeled cells among TIM4⁺ or TIM4⁻ cells in *Cx3cr1*^{CreER} X

607 *ROSA26*$^{LSL\text{-}GFP}$ embryos treated with 4-OHT at E9.5. **E** Scheme of the fate-

608 mapping experiments showing the relationship between *Cx3cr1*⁺ and *Timd4*⁺

609 thymic macrophages during embryonic development. E15.5 pregnant
610 *ROSA26*$^{LSL\text{-}GFP}$ mice mated with *Cx3cr1*^{CreER} males were injected with 4-
611 hydroxytamoxifen (4-OHT) and sacrificed at E19.5. **F** Representative flow
612 cytometry staining for TIM4 and CX3CR1 in fate-mapped GFP^{+} thymic
613 macrophages at E19.5. The panel to the right is the isotype control for
614 CX3CR1-PE staining. **G** Frequencies of TIM4^{+}CX3CR1^{-} cells among fate-
615 mapped GFP^{+} macrophages. Data are from at least two independent
616 experiments for each panel. Each symbol is an individual mouse or embryo.
617

618 ***Cx3cr1*$^{+}$ *thymic macrophages slowly accumulate with age at the***
619 ***expense of Timd4*$^{+}$ cells**

620 To understand the dynamics of the two resident thymic macrophage
621 populations with age, we induced recombination in *Cx3cr1*^{CreER} X *ROSA26*$^{LSL\text{-}}$
622 ^{GFP} mice during the neonatal period (Figure 8A) or at 6 weeks of age (Figure
623 8C) and compared the proportion of GFP^{+} cells 3 and 42 days after labeling.
624 The extent of labeling of TIM4^{+} thymic macrophages did not change within
625 these 6 weeks, no matter whether the mice were treated with Tamoxifen in
626 the first week after birth or at 6 weeks (Figure 8B and D), suggesting an
627 absence of a significant influx from unlabeled cells (e.g., monocytes). In
628 contrast, the proportion of labeled TIM4^{-} thymic macrophages decreased
629 significantly 6 weeks after Tamoxifen injection in neonatal and adult mice,
630 suggesting that this population was diluted by unlabeled cells. To further
631 substantiate these findings, we examined older WT mice and found out that
632 the proportions of TIM4^{-} thymic macrophages increased with age, and in mice
633 >8 months old, they accounted for ~70% of all macrophages in the organ

634 (Figure 8E). As these changes in the proportions of the thymic macrophage
635 subpopulations occurred at the background of thymic involution, we wanted to
636 know if the accumulation of TIM4⁻ cells was only relative or also in absolute
637 cell numbers. In contrast to TIM4⁺ thymic macrophages that reached peak
638 numbers at an early age and then declined significantly, TIM4⁻ cells tended to
639 increase their numbers in older mice (Figure 8F). Thus, we conclude that,
640 after birth, the numbers of TIM4⁺ macrophages follow the kinetics of the
641 thymus size – increase in young and decrease in old mice, and they are not
642 replaced by other cells. In contrast, since the first week of life, *Cx3cr1*⁺ cells
643 are recruited to the thymus, accumulate with age, and in old mice, form the
644 predominant phagocytic population in the organ.

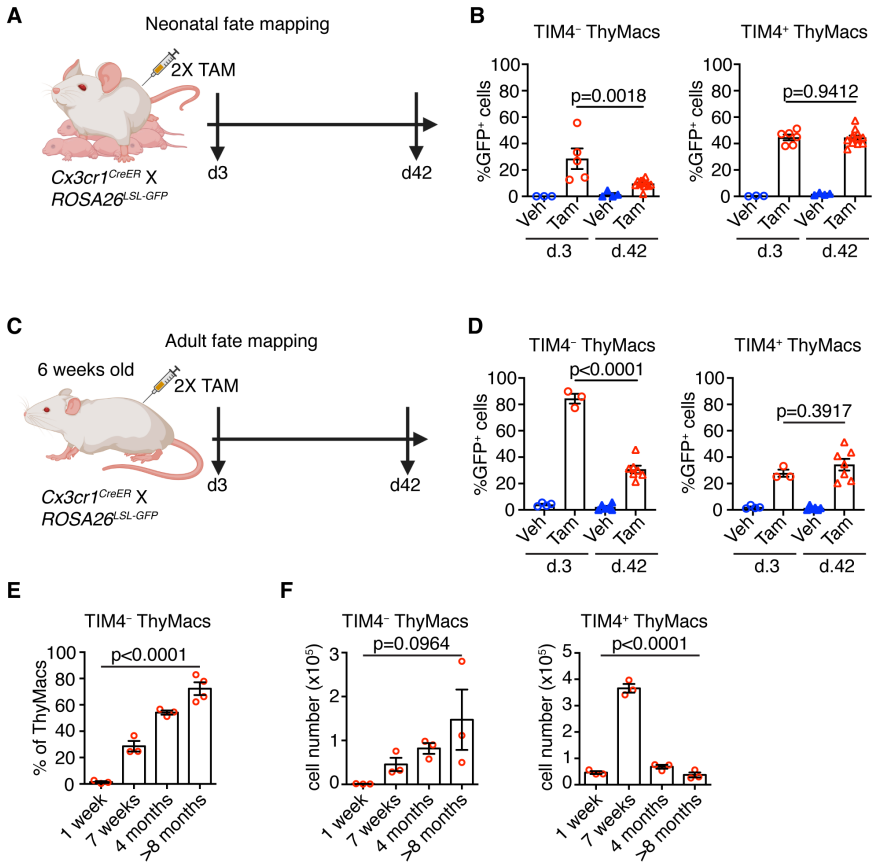

645

646 **Figure 8. *Timd4*⁺ thymic macrophages are progressively lost, while**
647 ***Cx3cr1*⁺ cells slowly accumulate with age. A** Scheme of the neonatal fate

648 mapping: A nursing dam was injected twice with Tamoxifen (Tam) or vehicle
649 (Veh) in the first week after giving birth to *Cx3cr1*^{CreER} X *ROSA26*$^{LSL\text{-}GFP}$ pups.
650 The mice were sacrificed three or 42 days after the last injection, and the
651 degree of labeling of TIM4^{+} and TIM4^{-} thymic macrophages was examined by
652 flow cytometry. **B** Frequencies of GFP^{+} TIM4^{+} or TIM4^{-} thymic macrophages
653 from neonatally fate-mapped mice after 3 and 42 days. Vehicle-injected
654 nursing dam litters (Veh) served as a control for non-specific labeling. **C**
655 Scheme of the adult fate mapping: Six weeks old *Cx3cr1*^{CreER} X *ROSA26*$^{LSL\text{-}}$
656 ^{GFP} mice were injected twice with Tamoxifen (Tam) or vehicle (Veh). The
657 mice were sacrificed three or 42 days after the last injection, and the degree
658 of labeling of TIM4^{+} and TIM4^{-} thymic macrophages was examined by flow
659 cytometry. **D** Frequencies of GFP^{+} TIM4^{+} or TIM4^{-} thymic macrophages from
660 adult fate-mapped mice after 3 and 42 days. **E** Frequencies of TIM4^{-} thymic
661 macrophages at different ages. **F** Changes in the numbers of TIM4^{-} and
662 TIM4^{+} thymic macrophages with age. The data are mean±SEM from 2
663 independent experiments (**B**) or at least 3 individual mice per time point (**D**,
664 **E**, and **F**). Each symbol is an individual mouse. Statistical significance in the
665 difference between Tamoxifen-treated samples at different time points was
666 determined with unpaired Student's t-test (**B** and **D**). One-way ANOVA was
667 used to assess the significance of the change in TIM4^{+} and TIM4^{-} ThyMacs
668 percentages and numbers with age (**E** and **F**).
669

670 **Discussion**

671 Here, we have described the phenotype, transcriptional profile, localization,
672 diversity, ontogeny, and maintenance of macrophages in the thymus. These

673 cells express the typical macrophage markers CD64, MerTK, and F4/80 and
674 are transcriptionally most similar to splenic red pulp macrophages and liver
675 Kupffer cells. However, they have a unique expression profile dominated by
676 genes involved in antigen presentation and lysosomal degradation. We found
677 that thymic macrophages consist of two populations with distinct localization.
678 *Timd4*$^{+}$ macrophages occupied the cortex, while *Cx3cr1*$^{+}$ cells were located in
679 the medulla and the cortico-medullary junction. While YS-derived
680 macrophages dominated the early stages of thymus development, they were
681 quickly replaced by non-YS embryonic progenitors that gave rise to the
682 *Timd4*$^{+}$ thymic macrophages that persisted into adulthood and formed the
683 main macrophage population in young mice. *Cx3cr1*$^{+}$ macrophages slowly
684 accumulated after birth and became the most abundant population in old
685 mice.
686 Altogether our data depict thymic macrophages as typical tissue-resident
687 macrophages originating from multiple hematopoietic waves, surviving long-
688 term, and expressing the core macrophage-specific genes. They are most
689 similar transcriptionally to splenic red pulp macrophages and Kupffer cells,
690 which is not surprising considering that they all specialize in efferocytosis and
691 have efficient lysosomal degradation machinery. These three populations
692 also shared expression of the transcription factor *Spic* that is induced by
693 heme released following red blood cells phagocytosis (Haldar et al., 2014).
694 However, the thymus is not known as a place for erythrocyte degradation.
695 Thus, the mechanism for *Spic* up-regulation in thymic macrophages is
696 unclear.

697 The unique features of thymic macrophages include high expression of
698 genes involved in the IFN-I pathway, antigen presentation, and lysosomal
699 degradation. The up-regulation of IFN-I-stimulated genes such as *Stat1*,
700 *Stat2*, *Irf7*, and *Irf8* can be explained by the constitutive secretion of IFN-I by
701 thymic epithelial cells (Lienenklaus et al., 2009) (Otero et al., 2013). The
702 purpose of IFN-I expression in the thymus in the absence of a viral infection is
703 unclear. Still, one possibility is that it mediates negative selection to IFN-
704 dependent genes as part of central tolerance.
705 Thymic macrophages highly express molecules involved in antigen
706 presentation, including MHC1 and MHC2, although the latter is expressed at
707 lower levels than in cDCs, and are functionally competent to induce T cell
708 activation. Thus, they have the potential to present antigens for both negative
709 selection and agonist selection. These two activities have traditionally been
710 assigned solely to cDCs (Breed et al., 2017). However, recent evidence
711 suggests that negative selection is most efficient when the cell that presents
712 the antigen to an auto-reactive thymocyte is also the one that phagocytoses it
713 (Kurd et al., 2019). So, macrophages' participation in thymocyte selection
714 needs to be re-evaluated.
715 The extraordinary ability of thymic macrophages to engulf and degrade
716 apoptotic thymocytes has been appreciated for a long time (Surh & Sprent,
717 1994), and our RNA-Seq data provides additional supporting evidence for this
718 function by highlighting the up-regulation of pathways involved in lysosomal
719 degradation. Moreover, we recently showed that the pentose phosphate
720 pathway has a central role in buffering the efferocytosis-associated oxidative
721 stress in thymic macrophages (Tsai et al., 2022). An interesting topic for future

722 research would be understanding how the metabolites derived from apoptotic
723 cells are returned to the microenvironment to support the proliferation of
724 immature thymocytes. A *SoLute Carrier* (*Slc*) genes-based program has been
725 described in vitro (Morioka et al., 2018), but its relevance to tissue-resident
726 macrophages remains to be determined. Altogether, our study demonstrates
727 that thymic macrophages are a unique subset of tissue-resident macrophages
728 and support the idea that resident macrophage phenotype is determined by
729 the combination of ontogeny, microenvironment, and other factors (Bleriot et
730 al., 2020).
731 Together with the study by Tacke et al., our work builds the following model
732 for thymic macrophage origin (Tacke et al., 2015): Thymic macrophages
733 develop in three distinct waves: YS-derived progenitors dominate the early
734 stages of thymus development but are replaced before birth by a second
735 wave of YS-independent embryonic progenitors that forms the bulk of thymic
736 macrophages after birth and can self-maintain into adulthood. With age, there
737 is a slow and steady influx of *Timd4*$^{-}$*Cx3cr1*$^{+}$ macrophage precursors that
738 occupy the medulla and cortico-medullary junction, becoming the major
739 phagocytic population in the thymus of older mice (>8 months). The second
740 wave of YS-independent macrophages is most likely the progeny of
741 embryonic HSCs based on *Flt3*^{Cre} fate mapping that showed that >80% of
742 thymic macrophages in adult mice are descendants of HSCs (Tacke et al.,
743 2015). Whether HSC-independent fetal liver monocytes contribute to thymic
744 macrophages and to what extent awaits the creation of models that can
745 specifically target this population of progenitors. Recruitment of circulating
746 monocytes to the resident macrophage pool in the thymus has been ruled out

747 previously by parabiosis and *Ccr2*$^{-/-}$ mice (Tacke et al., 2015). Our shield
748 chimera experiments have arrived at similar conclusions. However, the
749 relatively short duration of these experiments and their focus on the bulk
750 thymic macrophages have prevented the recognition of the gradual
751 accumulation of *Timd4*$^{-}$ macrophages. Once we zoomed in on this minor cell
752 population in young mice, the fate mapping clearly showed an influx of
753 unlabeled progenitors. Whether the progenitors of *Timd4*$^{-}$ macrophages are
754 monocytes remains to be formally demonstrated. However, monocytes have
755 been singled out as the source of all macrophage populations exhibiting
756 replacement in adults examined to date (Molawi et al., 2014; Goldmann et al.,
757 2016) (Jacome-Galarza et al., 2019) (Tamoutounour et al., 2013) (Bain et al.,
758 2014) (Bain et al., 2016). An alternative possibility involves thymocyte
759 progenitors that, under certain circumstances, have been shown to
760 differentiate into macrophages and granulocytes in the thymus (Wada et al.,
761 2008) (Bell & Bhandoola, 2008). However, if this occurs in unmanipulated mice
762 at a steady state remains unclear.
763 We observed interesting dynamics of the *Cx3cr1*$^{+}$ macrophages in the
764 thymus. Thymic macrophage progenitors are initially *Cx3cr1*$^{+}$ during the
765 embryonic period but gradually down-regulate this chemokine receptor and
766 up-regulate *Timd4* so that by day 7 after birth, there are almost no
767 *Cx3cr1*$^{+}$*Timd4*$^{-}$ cells remaining. *Cx3cr1*$^{+}$*Timd4*$^{-}$ macrophages start to
768 increase after the neonatal stage, but these cells come from an entirely
769 different source – adult hematopoietic cell-derived progenitors, and slowly
770 accumulate in the medulla with time so that by 6-8 months, they are the
771 majority of the resident macrophages in that tissue. Both YS-derived primitive

772 macrophages and fetal liver monocytes express *Cx3cr1* (Hoeffel et al., 2012)
773 (Mass et al., 2016). However, the tissue-resident macrophages in some organs
774 (e.g., Kupffer cells, alveolar macrophages, red pulp macrophages,
775 Langerhans cells) lose *Cx3cr1* expression similar to thymic macrophages,
776 while the macrophages in the intestines, aorta, kidney, dermis, lymph node T
777 cell zone, and microglia do not (Yona et al., 2013) (Tamoutounour et al., 2013)
778 (Ensan et al., 2015) (Baratin et al., 2017). Similar processes may occur in other
779 tissues where the embryonic macrophages transition to a *Cx3cr1*$^{-}$ phenotype
780 and are slowly replaced by monocyte-derived cells with age. However,
781 detailed time-course analyses of *Cx3cr1* expression starting before birth and
782 extending to very old (1 year) mice coupled with lineage tracing would be
783 necessary to document if this transition takes place.
784 The spatial segregation of the two macrophage populations in the thymus
785 implies that they might have distinct functions. *Timd4*$^{+}$ cells are restricted to
786 the cortex and are particularly abundant in the deeper cortex, close to the
787 medulla. Both positive and negative selection of thymocytes occur there, so
788 we speculate that *Timd4*$^{+}$ macrophages might be specialized in efferocytosis
789 of CD4^{+}CD8^{+} (double-positive) thymocytes that cannot interact with cortical
790 thymic epithelial cells and die by neglect or are auto-reactive and undergo
791 clonal deletion in the cortex (Stritesky et al., 2013). On the other hand,
792 *Cx3cr1*$^{+}$ macrophages accumulate in the medulla – the thymic region
793 specialized in negative selection to tissue-restricted antigens (TRA). They
794 might contribute to the process in several ways: 1) by carrying TRAs from
795 blood and peripheral organs. A similar process has been described for cDC2
796 (SIRPα^{+} DCs) (Bonasio et al., 2006; Baba et al., 2009). In fact, *Cx3cr1*$^{+}$ thymic

797 macrophages could have contributed to this role because they were not
798 distinguished from cDC2 in this study. 2) By capturing TRAs from *Aire*$^+$
799 medullary thymic epithelial cells and presenting them to auto-reactive
800 thymocytes as shown for DCs (Gallegos & Bevan, 2004) (Koble & Kyewski,
801 2009) (Vobořil et al., 2020). 3) By phagocytosing apoptotic TRA-specific
802 medullary thymocytes, a process we have observed before (Kurd et al., 2019).
803 The exact involvement of thymic macrophages in the selection events in the
804 thymus remains to be determined.
805 The accumulation of the *Cx3cr1*$^+$ cells in older mice has clear implications
806 for thymus aging. One key feature of thymus involution is the accumulation of
807 extracellular matrix produced by fibroblasts and the emergence of white
808 adipocytes (Dixit, 2012). A well-recognized driver of fibrosis is TGFβ1 (Budi et
809 al., 2021) that is induced by efferocytosis in macrophages (Huynh et al., 2002).
810 *Tgfb1* was highly expressed in thymic macrophages. However, its expression
811 was the highest in the *Timd4*$^+$ subset (Figure 4 – figure supplement 4). This
812 expression pattern casts some doubt that this molecule is the primary driver of
813 extracellular matrix accumulation during thymic involution because *Timd4*$^+$
814 macrophages peak in young mice (Fig. 8F). At that time, there is minimal
815 extracellular matrix in the cortex where these cells reside. In addition, during
816 thymic involution, the number of these cells declines significantly. The clear
817 correlation between the accumulation of *Cx3cr1*$^+$ thymic macrophages and
818 thymic involution suggests that some factor(s) produced exclusively by these
819 cells would be more relevant. For example, *Cx3cr1*$^+$ thymic macrophages are
820 the predominant producer of the growth factor PDGFα (Figure 4G) that is
821 required for the maintenance of adipocyte stem cells and can stimulate tissue

822 fibrosis (Rivera-Gonzalez et al., 2016) (Olson & Soriano, 2009). The gradual
823 accumulation of *Cx3cr1*$^{+}$ macrophages could increase the availability PDGFα
824 in the aging thymus stimulating extracellular matrix production and
825 differentiation of precursors into adipocytes. This model predicts that limiting
826 the influx of *Cx3cr1*$^{+}$ macrophage precursors could delay thymus involution.
827 Recent work described a novel phagocytic and antigen-presenting cell type
828 in the thymus called monocyte-derived DCs (Vobořil et al., 2020). The
829 phenotype of these cells overlaps with the CD64^{+}F4/80^{lo}CD11b^{+} cells in our
830 study. However, we favor the classification of these cells as monocytes based
831 on their expression of *Mafb*, CD64, and Ly6C and lack of expression of the
832 defining DC transcription factor *Zbtb46* (Figure 4B and D) (Satpathy et al.,
833 2012). As monocytes can differentiate into cDC2, particularly in the context of
834 inflammation (Guilliams et al., 2018), the precise identity and the relationship of
835 this population to thymic cDC2 remain to be established.
836 In the past several years, scRNA-Seq has come to the forefront of
837 biologists' efforts to disentangle the cellular diversity of tissues. Several
838 comprehensive studies have included samples from mouse or human thymus
839 (Han et al., 2018) (Tabula et al., 2018) (Tabula, 2020). However, too few thymic
840 macrophages were sampled in these studies to give meaningful clustering
841 results. Efforts specifically targeting the thymus have provided considerably
842 more information (Kernfeld et al., 2018) (Park et al., 2020), but macrophage
843 diversity was still not recognized. Characterization of rare populations such as
844 thymic macrophages (~0.1% of all cells in the thymus) requires optimized
845 enzymatic digestion procedures and enrichment strategies, as has already
846 been demonstrated for thymic epithelial cells (Bornstein et al., 2018) (Bautista

847 et al., 2021). Our scRNA-Seq dataset provides a rich resource for the
848 unbiased characterization of myeloid cells in the thymus and will greatly aid in
849 the understanding of the myeloid landscape of the thymus.
850 In summary, our work comprehensively characterizes macrophages in the
851 thymus and paves the way for the exploration of their functions.
852
853 **Materials and methods**
854 **Mice**
855 C57BL/6Narl (CD45.2) mice were purchased from the National Laboratory
856 Animal Center, Taipei, Taiwan (NLAC stock# RMRC11005). MAFIA
857 (MAcrophage Fas-Induced Apoptosis, Jackson Labs stock# 005070) (Burnett
858 et al., 2004), *Cx3cr1*^{GFP} (Jackson Labs stock# 005582) (Jung et al., 2000),
859 *Spic*^{GFP} (Jackson Labs stock# 025673) (Haldar et al., 2014), *Cx3cr1*^{CreER}
860 (Jackson Labs stock# 020940) (Yona et al., 2013), and *B6.SJL-Ptprca*
861 *Pepcb/BoyJ* (CD45.1, Jackson Labs stock# 002014) mice were purchased
862 from the Jackson Laboratories. *Cd11c*^{YFP} (Jackson Labs stock# 008829)
863 (Lindquist et al., 2004) and *Lyz2*^{GFP} (Faust et al., 2000) mice have been
864 described. Mice ubiquitously expressing GFP from the *ROSA26* locus were
865 generated by breeding *Pdgfra*^{Cre} (Jackson Labs stock# 013148) (Roesch et al.,
866 2008) and *ROSA26*$^{LSL\text{-}ZsGreen}$ (also known as *ROSA26*$^{LSL\text{-}GFP}$ or Ai6, Jackson
867 Labs stock# 007906) mice (Madisen et al., 2009) (both from the Jackson
868 Laboratories). A mouse from this cross was identified, in which the STOP
869 cassette was deleted in the germline. It was designated *ROSA26*^{GFP} and
870 subsequently bred to C57BL/6 mice. All mice were used at 4-10 weeks of age
871 unless otherwise specified. Mice were bred and maintained under specific

872 pathogen-free conditions at the animal facility of National Yang Ming Chiao
873 Tung University (NYCU). All experimental procedures were approved by the
874 Institutional Animal Care and Use Committee (IACUC) of NYCU.
875
876 **Treatment with 5-Ethynyl-2'-deoxyuridine (EdU)**
877 Mice were i.p. injected with 1 mg EdU (Carbosynth) dissolved in PBS daily
878 for 21 days and then rested for 21 more days. Cells from the thymus were
879 harvested on day 21 or 42. In some experiments, the mice were sacrificed 2
880 hours after the first EdU injection.
881
882 **Shield chimera generation**
883 WT (CD45.2) mice were anesthetized by i.p. injection of 120 μg/g body
884 weight Ketamine hydrochloride (Toronto Research Chemicals) and 12 μg/g
885 body weight Xylazine hydrochloride (Sigma). Anesthetized mice were taped
886 to a 5 cm thick lead block so that the lead block covered the head and the
887 chest down to the bottom of the rib cage. Then, they were irradiated with a
888 lethal dose (1000 rad) from a ^{137}Cs source (Minishot II, AXR) so that only their
889 abdomen and hind legs were exposed. After recovery from anesthesia, the
890 mice were transfused i.v. with 10^7 bone marrow cells from a congenic
891 (CD45.1) donor. Then, they were given Trimerin (0.5 mg/mL Sulfadiazine +
892 0.1 mg/mL Trimethoprim, China Chemical and Pharmaceutical Co., Tainan,
893 Taiwan) in the drinking water for the first two weeks after the irradiation and
894 analyzed after six weeks.
895
896 **Cell isolation from thymus, blood, and peritoneal cavity**

897 Thymocytes were obtained by mechanical disruption of the thymus with a
898 syringe plunger. For myeloid cell isolation, mouse thymuses were cut into
899 small pieces and digested with 0.2 mg/mL DNase I (Roche) and 0.2 mg/mL
900 collagenase P (Roche) in complete DMEM for 20 min at 37˚C with frequent
901 agitation. In some experiments, thymic myeloid cells were enriched by 57%
902 Percoll PLUS (GE Healthcare) discontinuous gradient centrifugation at 4˚C,
903 1800 rpm, for 20 min without brake. Cells at the interface were collected and
904 washed with PBS to remove residual silica particles. Then the cells were
905 resuspended in PBS with 0.5% BSA (HM Biological), filtered through a 70 μm
906 filter, and kept on ice.
907
908 Blood was isolated by cardiac puncture of sacrificed mice and immediately
909 diluted with PBS. After centrifugation, the cell suspensions were treated with
910 ammonium chloride-potassium lysis buffer for 3 min on ice once or twice.
911 Peritoneal cavity cells were obtained by lavage with 5 mL PBS + 2 mM EDTA
912 (Merck). Following gentle massage, the cavity was opened with an abdominal
913 incision, and lavage fluid was collected.
914
915 **Flow cytometry**
916 Single-cell suspensions (0.5 – 2X10^6 cells) from thymus, blood, or
917 peritoneal cavity were blocked with supernatant from 2.4G2 hybridoma (a kind
918 gift by Dr. Fang Liao, Academia Sinica, Taipei, Taiwan) and stained with
919 fluorochrome- or biotin-labeled antibodies for 20 min on ice in PBS + 0.5%
920 BSA + 2 mM EDTA + 0.1% NaN_3 (FACS buffer). The following antibodies
921 were used: CD11b (clone M1/70), MHC2 (M5/114.15.2), CD11c (N418),

922 F4/80 (BM8), CD115 (AFS98), SIRPα (P84), CD45 (30-F11), NK1.1 (PK136),
923 TIM4 (RMT4-54), Gr-1 (RB6-8C5), CD64 (X54-5/7.1), Siglec H (551), Ly6C
924 (HK1.4), CD3ε (145-2C11), CD8α (53-6.7), CD19 (6D5), B220 (RA3-6B2),
925 CD4 (GK1.5), CD51 (RMV-7), CD45.1 (A20), CD45.2 (104), CX3CR1
926 (SA011F11), and EpCAM (G8.8) from BioLegend; Axl (MAXL8DS), MerTK
927 (DS5MMER), and Ki67 (SolA15) were from eBioscience; Siglec F (E50-2440),
928 CD90.2 (30-H12), and CD11c (HL3) were from BD Biosciences. Cells were
929 washed, and if necessary, incubated for 20 more min with fluorochrome-
930 labeled Streptavidin: Streptavidin-AF647 (Jackson Immunoresearch) or
931 Streptavidin-APC/cy7, Streptavidin-BV421, Streptavidin-BV605 (BioLegend).
932 After the last wash, the cells were resuspended in FACS buffer containing
933 DAPI (BioLegend), Propidium Iodide (Sigma), or DRAQ7 (BioLegend) and
934 analyzed immediately on an LSR Fortessa flow cytometer running Diva 8
935 software (BD Biosciences). Typically, 500,000 cells were collected from
936 thymus samples. Data were analyzed using FlowJo software (TreeStar).
937
938 For intracellular staining, after surface antibody staining, the cells were
939 labeled with Zombie Aqua (BioLegend) for 30 min in ice. Then, the cells were
940 fixed with 2% paraformaldehyde (Electron Microscope Sciences) in PBS for
941 20 min on ice, permeabilized with either 0.5% Triton-X 100 (Sigma) for 20 min
942 on ice, or with Foxp3 staining kit (eBioscience) according to the protocol
943 provided by the manufacturer, and stained with antibodies for intracellular
944 markers for 40-60 min on ice.
945

946 For cell cycle analysis, 1-5x10^5 sorted thymic macrophages were fixed with
947 70% ethanol for 2 h on ice. The cells were spun down at 1800 rpm for 20 min
948 at 4˚C, washed with PBS, and stained with 1 μg/ml DAPI (BioLegend) for 30
949 min at room temperature in the dark.
950
951 For EdU staining, after surface marker and Zombie Aqua staining, cells
952 were fixed with 2% paraformaldehyde in PBS for 20 min on ice and
953 permeabilized with 0.5% Triton X-100 in PBS at room temperature for 20 min.
954 EdU was detected by adding an equal volume of 2X Click reaction buffer
955 consisting of 200 mM Tris, 200 mM ascorbic acid (Acros), 8 mM $CuSO_4$
956 (Acros), 8 μM Cy5-azide (Lumiprobe) to the permeabilized cells resuspended
957 in 0.5% Triton X-100 in PBS and incubation at room temperature for 30 min.
958 Cells were washed twice with 0.5% Triton X-100 in PBS and analyzed on a
959 flow cytometer.
960
961 **Cell sorting**
962 The sorting of thymic macrophages was done following the IMMGEN
963 guidelines. Briefly, the thymuses of 3 male C57BL/6Narl mice were harvested
964 in ice-cold staining buffer containing phenol red-free DMEM (Gibco) with 10
965 mM HEPES (Sigma), 0.1% NaN_3, and 2% FBS (Gibco). Single-cell
966 suspensions were prepared as described in the Flow cytometry section.
967 Percoll PLUS was used to enrich mononuclear cells. The cells were
968 resuspended at 10^8/mL in staining buffer and labeled with appropriate
969 antibodies for 15 min in ice. To sort thymic macrophages, the cells were first
970 labeled with biotinylated antibodies to lineage markers (Lin) – CD3, CD8, Gr1,

971 B220. After washing, the cells were stained with antibodies to CD11b, F4/80,
972 CD45, CD64, and Streptavidin-APC/cy7 for 15 min in ice. For sorting thymus
973 XCR1$^+$ and SIRPα^+ cDCs, antibodies to XCR1, SIRPα, CD11c, MHC2, CD64,
974 and F4/80 were used. For sorting peritoneal cavity macrophages, antibodies
975 to ICAM2 and F4/80 were used. Immediately before sorting, the dead cells
976 were excluded with DRAQ7 or PI. For RNA Sequencing experiments, the
977 cells were double-sorted on FACS Melody, or Aria cell sorters (BD
978 Biosciences) and 1000 cells were directly deposited in TCL buffer (Qiagen),
979 frozen in dry ice and sent to IMMGEN for RNA sequencing. Four biological
980 replicates were prepared. For cytospin and cell cycle analysis, 1-5x10^5 cells
981 sorted on FACS Melody were collected in staining buffer.
982
983 **Cytospin**
984 Sorted cells were mounted on Superfrost PLUS slides (Thermo Scientific)
985 using a Cytospin centrifuge (Cytospin 3, Shandon) for 5 min at 500 rpm. Cells
986 were fixed with 2% paraformaldehyde for 10 min at room temperature and
987 stained with the Hemacolor Rapid Staining Kit (Merck Millipore). Images were
988 collected on BX61 upright microscope (Olympus) using 100X objective with
989 immersion oil and captured with a CCD camera. Images were then analyzed
990 and processed with ImageJ (NIH) and Adobe Photoshop 5.5 (Adobe).
991
992 **In vitro phagocytosis assay**
993 10^7 Thymocytes were cultured in cDMEM in the presence of 1 μM of
994 dexamethasone (Sigma) in a 3.5-cm culture dish at 37℃ in 5% CO_2 incubator
995 for 8 hours. Apoptosis levels were assessed by PI (Biolegend) and Annexin V-

996 FITC (Biolegend) staining. Typically, more than 80% of cells were Annexin V^+.
997 The dexamethasone-treated thymocytes were stained with 1 μg/mL pHrodo
998 Red, SE (ThermoFisher) in PBS for 30 min at room temperature. The cells
999 were washed two times with cDMEM and resuspended at $2x10^6$ cells/mL.
1000 $4x10^4$ sorted peritoneal and thymic macrophages were stained with 5 μM
1001 eFluor 450 (Thermo Fisher) in PBS for 10 min at 37℃, washed two times with
1002 cDMEM and cultured in 96-well flat-bottom culture plate (Nunc) in 100 μL
1003 cDMEM at 37℃ in 5% CO_2 incubator. After 3 hours of attachment, the non-
1004 adherent cells were removed, and 200 μL ($4x10^5$) apoptotic thymocytes were
1005 added to the macrophages. The cells were incubated at 37℃ in 5% CO_2
1006 incubator for 2 hours. Fluorescent images were captured with AxioObserver 7
1007 (Carl Zeiss) wide-field microscope equipped with Plan Apochromat 40x
1008 NA=1.0 objective (Zeiss) and AxioCam 702 monochrome camera (Zeiss)
1009 controlled by Zen 2.3 Blue (Zeiss) software. Image analysis was performed
1010 with Imaris 8.0.2 (Bitplane). Phagocytosis was scored by investigators blinded
1011 to the samples' identities.
1012

1013 **In vitro antigen presentation assay**

1014 $3x10^4$ sorted thymic $CD64^-MHCII^+CD11c^+$ dendritic cells, thymic, or
1015 peritoneal macrophages were cultured in 96-well round-bottom culture plate in
1016 100 μL cDMEM at 37℃ in 5% CO_2 incubator for 3 hours to attach.
1017 Splenocytes from OT2 mice were stained with biotinylated antibodies to
1018 CD8a, CD11b, CD11c, B220, and MHCII (all from BioLegend), washed, and
1019 labeled with anti-biotin Microbeads (Miltenyi) plus CD44 microbeads (Miltenyi)
1020 in cRPMI. The cells were separated on MACS LS columns (Miltenyi)

1021 according to the manufacturer's instructions. Enriched cells (naïve CD4 T
1022 cells) were stained with 10 μM CFSE (Sigma) for 5 min in PBS at 37℃ and
1023 cocultured with the sorted thymic MHCII$^+$CD11c$^+$ dendritic cells, thymic, or
1024 peritoneal macrophages, in the presence or absence of 0.5 mg/mL OVA
1025 protein (Sigma) in cRPMI at 37℃ in 5% CO_2 incubator for 72 hours. The cells
1026 were collected and stained with antibodies to TCRβ and CD4 (from
1027 BioLegend) for flow cytometry analyses of CFSE dilution. The data were
1028 analyzed with FlowJo's Proliferation Modelling module (BD Biosciences).
1029

1030 **RNA sequencing analysis**

1031 RNA sequencing was done at IMMGEN using Smart-seq2 protocol (Picelli
1032 et al., 2013) (Picelli et al., 2014) on a NextSeq500 sequencer (Illumina).
1033 Following sequencing, raw reads were aligned with STAR to the mouse
1034 genome assembly mm10 and assigned to specific genes using the
1035 GENCODE vM12 annotation. Gene expression was normalized by DESeq2
1036 (Love et al., 2014) and visualized by Morpheus
1037 (https://software.broadinstitute.org/morpheus). The principal component
1038 analysis was done by plotPCA() function of R package "DESeq2. Gene
1039 expression of mouse transcription factors (Schmeier et al., 2017) was
1040 visualized in MultiplotStudio of GenePattern (Reich et al., 2006). GO
1041 enrichment was calculated and visualized in R by using clusterProfiler (Yu et
1042 al., 2012).
1043

1044 **Timed pregnancies and embryonic thymus analysis**

1045 To set up timed pregnancies, each male mouse (*Cx3cr1*$^{CreER/CreER}$,
1046 *Cx3cr1*$^{GFP/GFP}$ or C57BL/6) and female mouse (*ROSA26*$^{LSL\text{-}GFP/LSL\text{-}GFP}$ or
1047 C57BL/6) were housed together in the same cage for one night and separated
1048 on the next day, which we defined as embryonic day 0.5 (E0.5). Female mice
1049 were assumed to be pregnant if their weight gain was over 2 g at E8.5 (Heyne
1050 et al., 2015). Thymuses from E14.5 and E17.5 embryos, neonatal, 1-weeks-
1051 old pups, and adult mice (older than 6-weeks-old) were harvested,
1052 mechanically dissociated with plastic sticks in 1.5-mL centrifuge tubes, and
1053 enzymatically digested with 0.2 mg/mL DNase I and 0.2 mg/mL collagenase P
1054 in complete DMEM for 20 min at 37˚C with frequent agitation. The cells were
1055 resuspended in PBS with 0.5% BSA, filtered through a 70 μm filter, kept on
1056 ice, and used flow cytometric analysis as described in the Flow Cytometry
1057 section.
1058
1059 **Genetic fate mapping – E9.5, neonatal and adult**
1060 For genetic fate mapping, timed pregnancies of *Cx3cr1*$^{CreER/CreER}$ male and
1061 *ROSA26*$^{LSL\text{-}GFP/LSL\text{-}GFP}$ female mice were set up as described. To label the
1062 *Cx3cr1*$^{+}$ erythromyeloid progenitors derived from embryonic yolk sac (Mass et
1063 al., 2016), 4-hydroxytamoxifen (4-OHT from Sigma) was administered i.p. to
1064 pregnant females on E9.5 at a dose of 75 μg/g (body weight). To improve the
1065 survival of embryos and reduce the risk of abortions, Progesterone (Sigma)
1066 was co-injected at a dose of 37.5 μg/g (body weight) (Iturri et al., 2017). To
1067 label the *Cx3cr1*$^{+}$ thymic macrophages in *Cx3cr1*^{CreER} X *ROSA26*$^{LSL\text{-}GFP}$
1068 neonates and adult mice, Tamoxifen (TAM from Sigma) was injected i.p. at a
1069 dose of 2 mg/mouse to lactating dams on postnatal day 3 and 4 (P3 and P4)

1070 or to adult mice for 2 consecutive days. Thymuses were harvested and
1071 analyzed 3 days or 6 weeks after the last injection by flow cytometry.
1072
1073 **scRNA-Seq – sorting, library generation, and sequencing**
1074 scRNA-Seq was performed at the Genomics Center for Clinical and
1075 Biotechnological Applications of NCFB (NYCU, Taipei, Taiwan). Briefly, the
1076 thymuses of one female MAFIA and 2 male *Cd11c*^{YFP} mice were harvested
1077 and enzymatically digested as described previously. Mononuclear cells were
1078 enriched by 57% Percoll PLUS discontinuous centrifugation, washed to
1079 remove silica particles, and resuspended at 10^6/mL in PBS with 0.04% BSA.
1080 The cell suspensions were filtered through Falcon 35 μm strainer (Corning)
1081 and stained with viability dye (PI or DAPI) immediately before sorting. Cell
1082 sorting was performed on a FACS Melody sorter (BD Biosciences) running
1083 FACS Chorus (BD Biosciences) software in purity mode. $3X10^5$ GFP or YFP
1084 positive cells under the live/singlet gating were collected into 5 ml round
1085 bottom tubes pre-coated with 0.04% BSA in PBS. Sorted cells were washed
1086 and resuspended in 300 μL PBS with 0.04% BSA and then filtered again into
1087 1.5-mL DNA LoBind tubes (Eppendorf) through a 35 μm strainer. The viability
1088 of the cells was evaluated by Countess II (Invitrogen) and Trypan Blue
1089 (ThermoFisher), and samples with cell viability rates higher than 85% were
1090 used for encapsulation and library preparation. Single-cell encapsulation and
1091 library preparation were performed using Single Cell 3' v3/v3.1 Gene
1092 Expression solution (10x Genomics). All the libraries were processed
1093 according to the manufacturer's instruction and sequenced on NovaSeq 6000
1094 (Illumina) platform at the NHRI (Zhubei, Taiwan). Post-processing and quality

1095 control were performed by the NYCU Genome Center using the CellRanger
1096 package (v. 3.0.2, 10x Genomics). Reads were aligned to mm10 reference
1097 assembly. Primary assessment with CellRanger reported 9,973 cell-barcodes
1098 with 11,385 median unique molecular identifiers (UMIs, transcripts) per cell
1099 and 3,076 median genes per cell sequenced to 71.0% sequencing saturation
1100 with 94,260 mean reads per cell for MAFIA mouse sample; 9,801 cell-
1101 barcodes with 13,467 median UMIs per cell and 3,211 median genes per cell
1102 sequenced to 74.9% sequencing saturation with 119,820 mean reads per cell
1103 for the first *Cd11c*^{YFP} mouse sample; 12,938 cell-barcodes with 14,439
1104 median UMIs per cell and 3,199 median genes per cell sequenced to 71.4%
1105 sequencing saturation with 108,585 mean reads per cell for the second
1106 *Cd11c*^{YFP} mouse sample.
1107
1108 **Analysis of scRNA-Seq**
1109 Preprocessing
1110 The Scanpy (Wolf et al., 2018) pipeline was used to read the count matrix.
1111 Three batches of samples (one from GFP^{+} cells from MAFIA mouse and two
1112 from YFP^{+} cells from *Cd11c*^{YFP} mice) were preprocessed independently and
1113 integrated later. Cells that expressed <200 genes and genes that were
1114 expressed in <3 cells were filtered out. The percentage of mitochondrial
1115 genes was calculated -and cells with >10% mitochondrial genes were
1116 removed. Cells with >7,000 genes or <1,000 genes were also removed. Read
1117 counts were normalized to library size 10,000 and log-transformed with
1118 scanpy.pp.log1p function.
1119 Datasets integration and batch effect correction

1120 Read count matrices and spliced/unspliced matrices were merged first.
1121 Principal Component Analysis was applied to reduce dimensions to 70.
1122 BBKNN(Polański et al., 2020) was then used to remove batch effects with the
1123 scanpy.external.pp.bbknn function with default parameters.
1124 Visualization and clustering
1125 UMAP (McInnes et al., 2018) provided by scanpy was used to visualize data
1126 with default parameters. K-nearest neighbor and Leiden clustering were
1127 applied sequentially to cluster cells into groups. K-nearest neighbor graph
1128 construction was done by scanpy.pp.neighbors with parameters
1129 n_neighbors=12 and n_pcs=70. Leiden clustering was then performed by
1130 scanpy.tl.leiden with parameter resolution=0.15. To improve UMAP
1131 visualization, scanpy.tl.paga was applied, and we trimmed unnecessary graph
1132 edges by scanpy.tl.paga with threshold=0.018.
1133 Marker genes and statistics
1134 Wilcoxon rank-sum tests were applied to examine differentially expressed
1135 genes. Clusters were selected from the result of Leiden clustering.
1136 Differentially expressed genes of a cluster against other clusters were
1137 identified by scanpy.tl.rank_genes_groups and scanpy.pl.rank_genes_groups.
1138 P-values were collected for each cluster and transformed by negative $\log_{10}$ for
1139 better visualization. The top 50 differentially expressed genes were visualized
1140 in the figure.
1141
1142 **Immunofluorescent staining**
1143 Dissected thymus lobes from C57BL/6 mice were cleaned of connective
1144 tissue and fixed in 4% paraformaldehyde (Sigma) for 1 h at 4˚C, washed in

1145 PBS, submerged in 10% sucrose, and then in 30% sucrose for 12 h each.
1146 The tissue was then frozen in Tissue-Tek OCT compound (Sakura Fintek) for
1147 cryostat sectioning. 10 or 20 μm thick sections were prepared with CryoStar
1148 NX50 (ThermoFisher) on Superfrost PLUS (ThermoScientific) microscope
1149 slides, dried overnight, and stored at -80˚C until used. Before staining, the
1150 sections were fixed with acetone (Sigma) at -20˚C for 10 min, air-dried, then
1151 blocked with 5% goat serum + 5% donkey serum (both from Jackson
1152 Immunoresearch) in PBS for 2 h and stained with primary antibodies: rat
1153 monoclonal to MerTK (DS5MMER, eBioscience), rat monoclonal to TIM4
1154 (RMT4-54, Bio-X-Cell), rabbit polyclonal to CD64 (Sinobiological), or rabbit
1155 polyclonal to Keratin 5 (BioLegend) overnight at 4˚C in a humidified chamber.
1156 After washing in PBS, the sections were labeled with goat anti-rat-Alexa Fluor
1157 647 (Invitrogen) or goat anti-rat Cy3 (Jackson Immunoresearch) and donkey
1158 anti-rabbit Cy3 or donkey anti-rabbit AF647 (both from Jackson
1159 Immunoresearch) secondary antibodies for 2 hours at room temperature,
1160 followed by 5 min staining with DAPI. TUNEL Assay was done with the Click-
1161 iT Plus TUNEL Assay Alexa Fluor 647 kit (Invitrogen) according to the
1162 manufacturer's recommendations. A positive (pre-incubation with DNase I for
1163 30 min at room temperature) and negative (no TdT enzyme) controls were
1164 always included. The sections were mounted with 0.1% n-propyl gallate
1165 (Sigma) in glycerol (Sigma) and imaged with an AxioObserver 7 (Carl Zeiss)
1166 wide-field microscope equipped with Plan Apochromat 20x NA=0.8 objective
1167 (Zeiss) and AxioCam 702 mono camera (Zeiss) and controlled by Zen 2.3
1168 Blue (Zeiss) software. Image analysis was performed with Imaris 8.0.2
1169 (Bitplane).

1170

1171 The co-localization scoring for MerTK and TIM4 with TUNEL was done with
1172 Imaris 8.2 (Bitplane). TUNEL^{+} cells were detected with the Spots function,
1173 while MerTK^{+} and TIM4^{+} cells were detected with the Surface function. Spots
1174 that co-localize with Surfaces were identified with the “Find Spots close to
1175 Surface” function of Imaris XT. The threshold for co-localization was set to 5
1176 µm. The results were manually curated so that Spots categorized as “not co-
1177 localized” that were: 1) at the edge of the imaging field were excluded from
1178 consideration; 2) with clear Surface signal around them were re-categorized
1179 as "co-localized". The ratio of co-localized Spots to all Spots was calculated
1180 and presented as the co-localization index.

1181

1182 **Thymus transplantation**

1183 To obtain E15.5 embryos, *Spic*^{GFP} (CD45.2) homozygous male and
1184 congenic CD45.1 female mice were mated in a cage overnight and separated
1185 on the next day. Pregnant mice were sacrificed 15 days later, the viable
1186 embryos were harvested, and the thymuses were isolated in ice-cold PBS.
1187 C57BL/6 recipients were anesthetized by i.p injection of Ketamine
1188 hydrochloride (120 µg/g, Toronto Research Chemicals) and Xylazine
1189 hydrochloride (12 µg/g, Sigma). The fur on the left flank was removed, and the
1190 left kidney was exposed by cutting the skin, muscle layer, and peritoneum.
1191 The kidney capsule was nicked with a G23 needle, and the fetal thymus was
1192 pushed into the pocket under the kidney capsule with a G23 needle equipped
1193 with a plunger from a spinal needle. After the kidney was re-positioned back
1194 into the peritoneal cavity, the peritoneum was sutured, and the skin was

1195 stapled with metal clips. Rymadil (Carprofen, 5 μg/g, Zoetis) was given
1196 subcutaneously to ease the wound pain, and Trimerin (Sulfadiazine at 0.5
1197 mg/mL + Trimethoprim at 0.1 mg/mL) were given in the drinking water for the
1198 first two weeks after the surgery. The metal clips were removed from the skin
1199 after the first week, and the transplanted thymus and recipient's endogenous
1200 thymus were harvested and analyzed six weeks after the kidney
1201 transplantation.
1202
1203 **Statistical analysis**
1204 Comparison between groups was made with Prism 6 (GraphPad Software).
1205 Comparisons between two groups were carried out with unpaired Student's t-
1206 test. When more than two groups were compared, a one-way ANOVA with
1207 Tukey correction was used. Differences were considered significant if $p<0.05$.
1208
1209 **Data availability**
1210 The RNA Sequencing data of thymic macrophages and thymic dendritic
1211 cells are available at NCBI Gene Expression Omnibus (GEO) as part of
1212 GSE122108 and at www.immgen.org. The single cell RNA sequencing data is
1213 deposited at NCBI GEO under accession number GSE185460. The source
1214 data underlying Fig. 1G and H, Fig. 3B, D, and G, Fig. 5C, F, and I, Fig. 6B, E,
1215 G, and I, Fig. 7B, C, D, and G, Fig. 8B, D, E, and F, Fig. 1S4, Fig. 2S1, Fig.
1216 2S2, Fig. 2S3, Fig. 5S1, and Fig. 5S2 are provided in the Source Data files.
1217 All other data supporting the findings of this study are available within the
1218 article and its figures and tables.
1219

1220 **Abbreviations:**

1221 cDC – classical dendritic cell

1222 DC – dendritic cell

1223 EdU – 5-Ethynyl-2'-deoxyuridine

1224 GO – gene ontology

1225 HSC – hematopoietic stem cell

1226 IFN-I – type I Interferon

1227 IMMGEN – Immunological Genome Consortium

1228 scRNA-Seq – single-cell RNA sequencing

1229 TF – transcription factor

1230 ThyMacs – thymic macrophages

1231 TRA – tissue-restricted antigen

1232 YS – yolk sac

1233 **References:**

1234 A-Gonzalez, N., & Castrillo, A. (2018). Origin and Specialization of Splenic
1235 Macrophages. *Cellular Immunology*, *330*, 1-27.
1236 https://doi.org/10.1016/j.cellimm.2018.05.005
1237 Baba, T., Nakamoto, Y., & Mukaida, N. (2009). Crucial Contribution of Thymic
1238 Sirp + Conventional Dendritic Cells to Central Tolerance against Blood-Borne
1239 Antigens in a CCR2-Dependent Manner. *The Journal of Immunology*, *183*(5),
1240 3053-3063. https://doi.org/10.4049/jimmunol.0900438
1241 Bain, C. C., Bravo-Blas, A., Scott, C. L., Gomez Perdiguero, E., Geissmann, F.,
1242 Henri, S., Malissen, B., Osborne, L. C., Artis, D., & Mowat, A. M. (2014).
1243 Constant replenishment from circulating monocytes maintains the macrophage
1244 pool in the intestine of adult mice. *Nature immunology*, *15*(10), 929-937.
1245 https://doi.org/10.1038/ni.2967
1246 Bain, C. C., Hawley, C. A., Garner, H., Scott, C. L., Schridde, A., Steers, N. J., Mack,
1247 M., Joshi, A., Guilliams, M., Mowat, A. M. I., Geissmann, F., & Jenkins, S. J.
1248 (2016). Long-lived self-renewing bone marrow-derived macrophages displace
1249 embryo-derived cells to inhabit adult serous cavities. *Nature Communications*,
1250 *7*, 1-14. https://doi.org/10.1038/ncomms11852
1251 Baratin, M., Simon, L., Jorquera, A., Ghigo, C., Dembele, D., Nowak, J., Gentek, R.,
1252 Wienert, S., Klauschen, F., Malissen, B., Dalod, M., & Bajénoff, M. (2017). T
1253 Cell Zone Resident Macrophages Silently Dispose of Apoptotic Cells in the

Lymph Node. *Immunity*, *47*(2), 349-362.e5. https://doi.org/10.1016/j.immuni.2017.07.019

Bautista, J. L., Cramer, N. T., Miller, C. N., Chavez, J., Berrios, D. I., Byrnes, L. E., Germino, J., Ntranos, V., Sneddon, J. B., Burt, T. D., Gardner, J. M., Ye, C. J., Anderson, M. S., & Parent, A. V. (2021). Single-cell transcriptional profiling of human thymic stroma uncovers novel cellular heterogeneity in the thymic medulla. *Nat Commun*, *12*(1), 1096. https://doi.org/10.1038/s41467-021-21346-6

Bell, J. J., & Bhandoola, A. (2008). The earliest thymic progenitors for T cells possess myeloid lineage potential. *Nature*, *452*(7188), 764-767. https://doi.org/10.1038/nature06840

Bellomo, A., Gentek, R., Bajénoff, M., & Baratin, M. (2018). Lymph node macrophages_ Scavengers, immune sentinels and trophic effectors. *Cellular Immunology*, 1-7. https://doi.org/10.1016/j.cellimm.2018.01.010

Bleriot, C., Chakarov, S., & Ginhoux, F. (2020). Determinants of Resident Tissue Macrophage Identity and Function. *Immunity*, *52*(6), 957-970. https://doi.org/10.1016/j.immuni.2020.05.014

Bonasio, R., Scimone, M. L., Schaerli, P., Grabie, N., Lichtman, A. H., & Von Andrian, U. H. (2006). Clonal deletion of thymocytes by circulating dendritic cells homing to the thymus. *Nature immunology*, *7*(10), 1092-1100. https://doi.org/10.1038/ni1385

Bornstein, C., Nevo, S., Giladi, A., Kadouri, N., Pouzolles, M., Gerbe, F., David, E., Machado, A., Chuprin, A., Tóth, B., Goldberg, O., Itzkovitz, S., Taylor, N., Jay, P., Zimmermann, V. S., Abramson, J., & Amit, I. (2018). Single-cell mapping of the thymic stroma identifies IL-25-producing tuft epithelial cells. *Nature*, *559*(7715), 1-25. https://doi.org/10.1038/s41586-018-0346-1

Breed, E. R., Lee, S. T., & Hogquist, K. A. (2017). Directing T cell fate: How thymic antigen presenting cells coordinate thymocyte selection. *Seminars in Cell and Developmental Biology*, 1-9. https://doi.org/10.1016/j.semcdb.2017.07.045

Budi, E. H., Schaub, J. R., Decaris, M., Turner, S., & Derynck, R. (2021). TGF-β as a driver of fibrosis: physiological roles and therapeutic opportunities. *J Pathol*, *254*(4), 358-373. https://doi.org/10.1002/path.5680

Burnett, S. H., Kershen, E. J., Zhang, J., Zeng, L., Straley, S. C., Kaplan, A. M., & Cohen, D. A. (2004). Conditional macrophage ablation in transgenic mice expressing a Fas-based suicide gene. *Journal of Leukocyte Biology*, *75*(4), 612-623. https://doi.org/10.1189/jlb.0903442

Calderon, B., Carrero, J. A., Ferris, S. T., Sojka, D. K., Moore, L., Epelman, S., Murphy, K. M., Yokoyama, W. M., Randolph, G. J., & Unanue, E. R. (2015). The pancreas anatomy conditions the origin and properties of resident macrophages. *J Exp Med*, *212*(10), 1497-1512. https://doi.org/10.1084/jem.20150496

Chan, C. T., Fenn, A. M., Harder, N. K., Mindur, J. E., McAlpine, C. S., Patel, J., Valet, C., Rattik, S., Iwamoto, Y., He, S., Anzai, A., Kahles, F., Poller, W. C., Janssen, H., Wong, L. P., Fernandez-Hernando, C., Koolbergen, D. R., van der Laan, A. M., Yvan-Charvet, L., . . . Swirski, F. K. (2020). Liver X receptors are required for thymic resilience and T cell output. *The Journal of experimental medicine*, *217*(10), 245-223. https://doi.org/10.1084/jem.20200318

Dixit, V. D. (2012). Impact of immune-metabolic interactions on age-related thymic demise and T cell senescence. *Seminars in Immunology*, *24*(5), 321-330. https://doi.org/10.1016/j.smim.2012.04.002

Ebihara, T., Song, C., Ryu, S. H., Plougastel-Douglas, B., Yang, L., Levanon, D., Groner, Y., Bern, M. D., Stappenbeck, T. S., Colonna, M., Egawa, T., & Yokoyama, W. M. (2015). Runx3 specifies lineage commitment of innate lymphoid cells. *Nature immunology*, *16*(11), 1124-1133. https://doi.org/10.1038/ni.3272

Ensan, S., Li, A., Besla, R., Degousee, N., Cosme, J., Roufaiel, M., Shikatani, E. A., El-Maklizi, M., Williams, J. W., Robins, L., Li, C., Lewis, B., Yun, T. J., Lee, J. S., Wieghofer, P., Khattar, R., Farrokhi, K., Byrne, J., Ouzounian, M., . . . Robbins, C. S. (2015). Self-renewing resident arterial macrophages arise from embryonic CX3CR1+ precursors and circulating monocytes immediately after birth. *Nature immunology*, *17*(2), 159-168. https://doi.org/10.1038/ni.3343

Epelman, S., Lavine, K. J., Beaudin, A. E., Sojka, D. K., Carrero, J. A., Calderon, B., Brija, T., Gautier, E. L., Ivanov, S., Satpathy, A. T., Schilling, J. D., Schwendener, R., Sergin, I., Razani, B., Forsberg, E. C., Yokoyama, W. M., Unanue, E. R., Colonna, M., Randolph, G. J., . . . Mann, D. L. (2014). Embryonic and Adult-Derived Resident Cardiac Macrophages Are Maintained through Distinct Mechanisms at Steady State and during Inflammation. *Immunity*, *40*(1), 91-104. https://doi.org/10.1016/j.immuni.2013.11.019

Esashi, E., Sekiguchi, T., Ito, H., Koyasu, S., & Miyajima, A. (2003). Cutting Edge: A possible role for CD4+ thymic macrophages as professional scavengers of apoptotic thymocytes. *Journal of immunology (Baltimore, Md : 1950)*, *171*(6), 2773-2777. https://doi.org/10.4049/jimmunol.171.6.2773

Fainaru, O., Woolf, E., Lotem, J., Yarmus, M., Brenner, O., Goldenberg, D., Negreanu, V., Bernstein, Y., Levanon, D., Jung, S., & Groner, Y. (2004). Runx3 regulates mouse TGF-beta-mediated dendritic cell function and its absence results in airway inflammation. *EMBO J*, *23*(4), 969-979. https://doi.org/10.1038/sj.emboj.7600085

Faust, N., Varas, F., Kelly, L. M., Heck, S., & Graf, T. (2000). Insertion of enhanced green fluorescent protein into the lysozyme gene creates mice with green fluorescent granulocytes and macrophages. *Blood*, *96*(2), 719-726. http://eutils.ncbi.nlm.nih.gov/entrez/eutils/elink.fcgi?dbfrom=pubmed&id=10887140&retmode=ref&cmd=prlinks

Gallegos, A. M., & Bevan, M. J. (2004). Central Tolerance to Tissue-specific Antigens Mediated by Direct and Indirect Antigen Presentation. *The Journal of experimental medicine*, *200*(8), 1039-1049. https://doi.org/10.1084/jem.20041457

Gautier, E. L., Shay, T., Miller, J., Greter, M., Jakubzick, C., Ivanov, S., Helft, J., Chow, A., Elpek, K. G., Gordonov, S., Mazloom, A. R., Ma'ayan, A., Chua, W.-J., Hansen, T. H., Turley, S. J., Merad, M., Randolph, G. J., & Consortium, I. G. (2012). Gene-expression profiles and transcriptional regulatory pathways that underlie the identity and diversity of mouse tissue macrophages. *Nature immunology*, *13*(11), 1118-1128. https://doi.org/10.1038/ni.2419

Ginhoux, F., Greter, M., Leboeuf, M., Nandi, S., See, P., Gokhan, S., Mehler, M. F., Conway, S. J., Ng, L. G., Stanley, E. R., Samokhvalov, I. M., & Merad, M. (2010). Fate mapping analysis reveals that adult microglia derive from primitive macrophages. *Science (New York, NY)*, *330*(6005), 841-845. https://doi.org/10.1126/science.1194637

Ginhoux, F., & Guilliams, M. (2016). Tissue-Resident Macrophage Ontogeny and Homeostasis. *Immunity*, *44*(3), 439-449. https://doi.org/10.1016/j.immuni.2016.02.024

Goldmann, T., Wieghofer, P., Jordão, M. J. C., Prutek, F., Hagemeyer, N., Frenzel, K., Amann, L., Staszewski, O., Kierdorf, K., Krueger, M., Locatelli, G., Hochgerner, H., Zeiser, R., Epelman, S., Geissmann, F., Priller, J., Rossi, F. M. V., Bechmann, I., Kerschensteiner, M., . . . Prinz, M. (2016). Origin, fate and dynamics of macrophages at central nervous system interfaces. *Nature immunology*, *17*(7), 797-805. https://doi.org/10.1038/ni.3423

Guerri, L., Peguillet, I., Geraldo, Y., Nabti, S., Premel, V., & Lantz, O. (2013). Analysis of APC types involved in CD4 tolerance and regulatory T cell generation using reaggregated thymic organ cultures. *The Journal of Immunology*, *190*(5), 2102-2110. https://doi.org/10.4049/jimmunol.1202883

Guilliams, M., Mildner, A., & Yona, S. (2018). Developmental and Functional Heterogeneity of Monocytes. *Immunity*, *49*(4), 595-613. https://doi.org/10.1016/j.immuni.2018.10.005

Haldar, M., Kohyama, M., So, A. Y.-L., KC, W., Wu, X., Briseño, C. G., Satpathy, A. T., Kretzer, N. M., Arase, H., Rajasekaran, N. S., Wang, L., Egawa, T., Igarashi, K., Baltimore, D., Murphy, T. L., & Murphy, K. M. (2014). Heme-Mediated SPI-C Induction Promotes Monocyte Differentiation into Iron-Recycling Macrophages. *Cell*, *156*(6), 1223-1234. https://doi.org/10.1016/j.cell.2014.01.069

Han, X., Wang, R., Zhou, Y., Fei, L., Sun, H., Lai, S., Saadatpour, A., Zhou, Z., Chen, H., Ye, F., Huang, D., Xu, Y., Huang, W., Jiang, M., Jiang, X., Mao, J., Chen, Y., Lu, C., Xie, J., . . . Guo, G. (2018). Mapping the Mouse Cell Atlas by Microwell-Seq. *Cell*, *172*(5), 1091-1107.e17. https://doi.org/10.1016/j.cell.2018.02.001

Hashimoto, D., Chow, A., Noizat, C., Teo, P., Beasley, M. B., Leboeuf, M., Becker, C. D., See, P., Price, J., Lucas, D., Greter, M., Mortha, A., Boyer, S. W., Forsberg, E. C., Tanaka, M., van Rooijen, N., García-Sastre, A., Stanley, E. R., Ginhoux, F., . . . Merad, M. (2013). Tissue-Resident Macrophages Self-Maintain Locally throughout Adult Life with Minimal Contribution from Circulating Monocytes. *Immunity*, *38*(4), 792-804. https://doi.org/10.1016/j.immuni.2013.04.004

Heidt, T., Courties, G., Dutta, P., Sager, H. B., Sebas, M., Iwamoto, Y., Sun, Y., Da Silva, N., Panizzi, P., van der Laan, A. M., Swirski, F. K., Weissleder, R., & Nahrendorf, M. (2014). Differential Contribution of Monocytes to Heart Macrophages in Steady-State and After Myocardial Infarction. *Circulation Research*, *115*(2), 284-295. https://doi.org/10.1161/CIRCRESAHA.115.303567

Heyne, G. W., Plisch, E. H., Melberg, C. G., Sandgren, E. P., Peter, J. A., & Lipinski, R. J. (2015). A Simple and Reliable Method for Early Pregnancy Detection in Inbred Mice. *Journal of the American Association for Laboratory Animal Science : JAALAS*, *54*(4), 368-371. http://eutils.ncbi.nlm.nih.gov/entrez/eutils/elink.fcgi?dbfrom=pubmed&id=26224435&retmode=ref&cmd=prlinks

Hoeffel, G., Chen, J., Lavin, Y., Low, D., Almeida, F. F., See, P., Beaudin, A. E., Lum, J., Low, I., Forsberg, E. C., Poidinger, M., Zolezzi, F., Larbi, A., Ng, L. G., Chan, J. K. Y., Greter, M., Becher, B., Samokhvalov, I. M., Merad, M., . . . Ginhoux, F. (2015). C-Myb(+) erythro-myeloid progenitor-derived fetal

monocytes give rise to adult tissue-resident macrophages. *Immunity*, *42*(4), 665-678. https://doi.org/10.1016/j.immuni.2015.03.011

Hoeffel, G., Wang, Y., Greter, M., See, P., Teo, P., Malleret, B., Leboeuf, M., Low, D., Oller, G., Almeida, F., Choy, S. H. Y., Grisotto, M., Renia, L., Conway, S. J., Stanley, E. R., Chan, J. K. Y., Ng, L. G., Samokhvalov, I. M., Merad, M., . . . Ginhoux, F. (2012). Adult Langerhans cells derive predominantly from embryonic fetal liver monocytes with a minor contribution of yolk sac–derived macrophages. *The Journal of experimental medicine*, *209*(6), 1167-1181. https://doi.org/10.1084/jem.20120340

Hume, D. A. (2011). Applications of myeloid-specific promoters in transgenic mice support in vivo imaging and functional genomics but do not support the concept of distinct macrophage and dendritic cell lineages or roles in immunity. *Journal of Leukocyte Biology*, *89*(4), 525-538. https://doi.org/10.1189/jlb.0810472

Huynh, M. L., Fadok, V. A., & Henson, P. M. (2002). Phosphatidylserine-dependent ingestion of apoptotic cells promotes TGF-beta1 secretion and the resolution of inflammation. *J Clin Invest*, *109*(1), 41-50. https://doi.org/10.1172/JCI11638

Ingersoll, M. A., Spanbroek, R., Lottaz, C., Gautier, E. L., Frankenberger, M., Hoffmann, R., Lang, R., Haniffa, M., Collin, M., Tacke, F., Habenicht, A. J. R., Ziegler-Heitbrock, L., & Randolph, G. J. (2010). Comparison of gene expression profiles between human and mouse monocyte subsets. *Blood*, *115*(3), e10-e19. https://doi.org/10.1182/blood-2009-07-235028

Iturri, L., Saenz Coronilla, J., Lallemand, Y., & Gomez Perdiguero, E. (2017). Identification Of Erythromyeloid Progenitors And Their Progeny In The Mouse Embryo By Flow Cytometry. *Journal of Visualized Experiments*, 125), 1-10. https://doi.org/10.3791/55305

Jacome-Galarza, C. E., Percin, G. I., Muller, J. T., Mass, E., Lazarov, T., Eitler, J., Rauner, M., Yadav, V. K., Crozet, L., Bohm, M., Loyher, P. L., Karsenty, G., Waskow, C., & Geissmann, F. (2019). Developmental origin, functional maintenance and genetic rescue of osteoclasts. *Nature*, *568*(7753), 541-545. https://doi.org/10.1038/s41586-019-1105-7

Jung, S., Aliberti, J., Graemmel, P., Sunshine, M. J., Kreutzberg, G. W., Sher, A., & Littman, D. R. (2000). Analysis of fractalkine receptor CX(3)CR1 function by targeted deletion and green fluorescent protein reporter gene insertion. *Molecular and cellular biology*, *20*(11), 4106-4114. http://eutils.ncbi.nlm.nih.gov/entrez/eutils/elink.fcgi?dbfrom=pubmed&id=10805752&retmode=ref&cmd=prlinks

Kernfeld, E. M., Genga, R. M. J., Neherin, K., Magaletta, M. E., Xu, P., & Maehr, R. (2018). A Single-Cell Transcriptomic Atlas of Thymus Organogenesis Resolves Cell Types and Developmental Maturation. *Immunity*, 1-33. https://doi.org/10.1016/j.immuni.2018.04.015

Kim, H.-J., Alonzo, E. S., Dorothee, G., Pollard, J. W., & Sant'Angelo, D. B. (2010). Selective depletion of eosinophils or neutrophils in mice impacts the efficiency of apoptotic cell clearance in the thymus. *PloS one*, *5*(7), e11439. https://doi.org/10.1371/journal.pone.0011439.g010

Koble, C., & Kyewski, B. (2009). The thymic medulla: a unique microenvironment for intercellular self-antigen transfer. *The Journal of experimental medicine*, *206*(7), 1505-1513. https://doi.org/10.1084/jem.20082449

Kohyama, M., Ise, W., Edelson, B. T., Wilker, P. R., Hildner, K., Mejia, C., Frazier, W. A., Murphy, T. L., & Murphy, K. M. (2008). Role for Spi-C in the

development of red pulp macrophages and splenic iron homeostasis. *Nature Immunology*, *457*(7226), 318-321. https://doi.org/10.1038/nature07472

Kurd, N. S., Lutes, L. K., Yoon, J., Chan, S. W., Dzhagalov, I. L., Hoover, A. R., & Robey, E. A. (2019). A role for phagocytosis in inducing cell death during thymocyte negative selection. *eLife*, *8*, 1879-1818. https://doi.org/10.7554/eLife.48097

Lienenklaus, S., Cornitescu, M., Zietara, N., Łyszkiewicz, M., Gekara, N., Jabłónska, J., Edenhofer, F., Rajewsky, K., Bruder, D., Hafner, M., Staeheli, P., & Weiss, S. (2009). Novel reporter mouse reveals constitutive and inflammatory expression of IFN-beta in vivo. *J Immunol*, *183*(5), 3229-3236. https://doi.org/10.4049/jimmunol.0804277

Lindquist, R. L., Shakhar, G., Dudziak, D., Wardemann, H., Eisenreich, T., Dustin, M. L., & Nussenzweig, M. C. (2004). Visualizing dendritic cell networks in vivo. *Nature immunology*, *5*(12), 1243-1250. https://doi.org/10.1038/ni1139

Liu, L.-T., Lang, Z.-F., Li, Y., Zhu, Y.-J., Zhang, J.-T., Guo, S.-F., Wang, J.-X., Wang, H.-W., & Xu, Y.-D. (2013). Composition and characteristics of distinct macrophage subpopulations in the mouse thymus. *Molecular Medicine Reports*, *7*(6), 1850-1854. https://doi.org/10.3892/mmr.2013.1448

Liu, Z., Gu, Y., Chakarov, S., Bleriot, C., Kwok, I., Chen, X., Shin, A., Huang, W., Dress, R. J., Dutertre, C.-A., Schlitzer, A., Chen, J., Ng, L. G., Wang, H., Liu, Z., Su, B., & Ginhoux, F. (2019). Fate Mapping via Ms4a3-Expression History Traces Monocyte-Derived Cells. *Cell*, *178*(6), 1509-1525.e19. https://doi.org/10.1016/j.cell.2019.08.009

Lokka, E., Lintukorpi, L., Cisneros-Montalvo, S., Mäkelä, J.-A., Tyystjärvi, S., Ojasalo, V., Gerke, H., Toppari, J., Rantakari, P., & Salmi, M. (2020). Generation, localization and functions of macrophages during the development of testis. *Nature Communications*, *11*(1), 1-16. https://doi.org/10.1038/s41467-020-18206-0

Lopes, N., Charaix, J., Cédile, O., Sergé, A., & Irla, M. (2018). Lymphotoxin alpha fine-tunes T cell clonal deletion by regulating thymic entry of antigen-presenting cells. *Nature Communications*, *9*(1), 1-16. https://doi.org/10.1038/s41467-018-03619-9

Love, M. I., Huber, W., & Anders, S. (2014). Moderated estimation of fold change and dispersion for RNA-seq data with DESeq2. *Genome Biology*, *15*(12), 31-21. https://doi.org/10.1186/s13059-014-0550-8

Madisen, L., Zwingman, T. A., Sunkin, S. M., Oh, S. W., Zariwala, H. A., Gu, H., Ng, L. L., Palmiter, R. D., Hawrylycz, M. J., Jones, A. R., Lein, E. S., & Zeng, H. (2009). A robust and high-throughput Cre reporting and characterization system for the whole mouse brain. *Nature Neuroscience*, *13*(1), 133-140. https://doi.org/10.1038/nn.2467

Mass, E., Ballesteros, I., Farlik, M., Halbritter, F., Günther, P., Crozet, L., Jacome-Galarza, C. E., Händler, K., Klughammer, J., Kobayashi, Y., Gomez Perdiguero, E., Schultze, J. L., Beyer, M., Bock, C., & Geissmann, F. (2016). Specification of tissue-resident macrophages during organogenesis. *Science (New York, NY)*, *353*(6304), aaf4238-aaf4238. https://doi.org/10.1126/science.aaf4238

McInnes, L., Healy, J., & Melville, J. (2018). UMAP: Uniform Manifold Approximation and Projection for Dimension Reduction. *arXiv*, 1802.03426v3. http://arxiv.org/abs/1802.03426v3

http://arxiv.org/pdf/1802.03426v3

Molawi, K., Wolf, Y., Kandalla, P. K., Favret, J., Hagemeyer, N., Frenzel, K., Pinto, A. R., Klapproth, K., Henri, S., Malissen, B., Rodewald, H.-R., Rosenthal, N. A., Bajénoff, M., Prinz, M., Jung, S., & Sieweke, M. H. (2014). Progressive replacement of embryo-derived cardiac macrophages with age. *The Journal of experimental medicine*, *211*(11), 2151-2158. https://doi.org/10.1084/jem.20140639

Mondor, I., Baratin, M., Lagueyrie, M., Saro, L., Henri, S., Gentek, R., Suerinck, D., Kastenmuller, W., Jiang, J. X., & Bajénoff, M. (2019). Lymphatic Endothelial Cells Are Essential Components of the Subcapsular Sinus Macrophage Niche. *Immunity*, *50*(6), 1453-1466.e4. https://doi.org/10.1016/j.immuni.2019.04.002

Morioka, S., Perry, J. S. A., Raymond, M. H., Medina, C. B., Zhu, Y., Zhao, L., Serbulea, V., Onengut-Gumuscu, S., Leitinger, N., Kucenas, S., Rathmell, J. C., Makowski, L., & Ravichandran, K. S. (2018). Efferocytosis induces a novel SLC program to promote glucose uptake and lactate release. *Nature*, *563*(7733), 1-21. https://doi.org/10.1038/s41586-018-0735-5

Mossadegh-Keller, N., Gentek, R., Gimenez, G., Bigot, S., Mailfert, S., & Sieweke, M. H. (2017). Developmental origin and maintenance of distinct testicular macrophage populations. *The Journal of experimental medicine*, *214*(10), 2829-2841. https://doi.org/10.1084/jem.20170829

Olson, L. E., & Soriano, P. (2009). Increased PDGFRalpha activation disrupts connective tissue development and drives systemic fibrosis. *Dev Cell*, *16*(2), 303-313. https://doi.org/10.1016/j.devcel.2008.12.003

Otero, D. C., Baker, D. P., & David, M. (2013). IRF7-Dependent IFN-β Production in Response to RANKL Promotes Medullary Thymic Epithelial Cell Development. *The Journal of Immunology*, *190*(7), 3289-3298. https://doi.org/10.4049/jimmunol.1203086

Park, J.-E., Botting, R. A., Domínguez Conde, C., Popescu, D.-M., Lavaert, M., Kunz, D. J., Goh, I., Stephenson, E., Ragazzini, R., Tuck, E., Wilbrey-Clark, A., Roberts, K., Kedlian, V. R., Ferdinand, J. R., He, X., Webb, S., Maunder, D., Vandamme, N., Mahbubani, K. T., . . . Teichmann, S. A. (2020). A cell atlas of human thymic development defines T cell repertoire formation. *Science (New York, NY)*, *367*(6480), eaay3224-12. https://doi.org/10.1126/science.aay3224

Perdiguero, E. G., & Geissmann, F. (2015). The development and maintenance of resident macrophages. *Nature Immunology*, *17*(1), 2-8. https://doi.org/10.1038/ni.3341

Picelli, S., Björklund, Å. K., Faridani, O. R., Sagasser, S., Winberg, G., & Sandberg, R. (2013). Smart-seq2 for sensitive full-length transcriptome profiling in single cells. *Nature Methods*, *10*(11), 1096-1098. https://doi.org/10.1038/nmeth.2639

Picelli, S., Faridani, O. R., rklund, A. S. K. B. O., Winberg, G. O. S., Sagasser, S., & Sandberg, R. (2014). Full-length RNA-seq from single cells using Smart-seq2. *Nature protocols*, *9*(1), 171-181. https://doi.org/10.1038/nprot.2014.006

Polański, K., Young, M. D., Miao, Z., Meyer, K. B., Teichmann, S. A., & Park, J. E. (2020). BBKNN: fast batch alignment of single cell transcriptomes. *Bioinformatics*, *36*(3), 964-965. https://doi.org/10.1093/bioinformatics/btz625

Reich, M., Liefeld, T., Gould, J., Lerner, J., Tamayo, P., & Mesirov, J. P. (2006). GenePattern 2.0. *Nature genetics*, *38*(5), 500-501. https://doi.org/10.1038/ng0506-500

Rivera-Gonzalez, G. C., Shook, B. A., Andrae, J., Holtrup, B., Bollag, K., Betsholtz, C., Rodeheffer, M. S., & Horsley, V. (2016). Skin Adipocyte Stem Cell Self-

Renewal Is Regulated by a PDGFA/AKT-Signaling Axis. *Cell Stem Cell*, *19*(6), 738-751. https://doi.org/10.1016/j.stem.2016.09.002

Roesch, K., Jadhav, A. P., Trimarchi, J. M., Stadler, M. B., Roska, B., Sun, B. B., & Cepko, C. L. (2008). The transcriptome of retinal Müller glial cells. *The Journal of comparative neurology*, *509*(2), 225-238. https://doi.org/10.1002/cne.21730

Sasmono, R. T., Oceandy, D., Pollard, J. W., Tong, W., Pavli, P., Wainwright, B. J., Ostrowski, M. C., Himes, S. R., & Hume, D. A. (2003). A macrophage colony-stimulating factor receptor-green fluorescent protein transgene is expressed throughout the mononuclear phagocyte system of the mouse. *Blood*, *101*(3), 1155-1163. https://doi.org/10.1182/blood-2002-02-0569

Satpathy, A. T., KC, W., Albring, J. C., Edelson, B. T., Kretzer, N. M., Bhattacharya, D., Murphy, T. L., & Murphy, K. M. (2012). Zbtb46expression distinguishes classical dendritic cells and their committed progenitors from other immune lineages. *The Journal of experimental medicine*, *209*(6), 1135-1152. https://doi.org/10.1084/jem.20120030

Schlenner, S. M., Madan, V., Busch, K., Tietz, A., LAufle, C., Costa, C., Blum, C., Fehling, H. J. O., & Rodewald, H.-R. (2010). Fate Mapping Reveals Separate Origins of T Cells and Myeloid Lineages in the Thymus. *Immunity*, *32*(3), 426-436. https://doi.org/10.1016/j.immuni.2010.03.005

Schmeier, S., Alam, T., Essack, M., & Bajic, V. B. (2017). TcoF-DB v2: update of the database of human and mouse transcription co-factors and transcription factor interactions. *Nucleic acids research*, *45*(D1), D145-D150. https://doi.org/10.1093/nar/gkw1007

Sheng, J., Ruedl, C., & Karjalainen, K. (2015). Most Tissue-Resident Macrophages Except Microglia Are Derived from Fetal Hematopoietic Stem Cells. *Immunity*, *43*(2), 382-393. https://doi.org/10.1016/j.immuni.2015.07.016

Sierro, F., Evrard, M., Rizzetto, S., Melino, M., Mitchell, A. J., Florido, M., Beattie, L., Walters, S. B., Tay, S. S., Lu, B., Holz, L. E., Roediger, B., Wong, Y. C., Warren, A., Ritchie, W., McGuffog, C., Weninger, W., Le Couteur, D. G., Ginhoux, F., . . . Bertolino, P. (2017). A Liver Capsular Network of Monocyte-Derived Macrophages Restricts Hepatic Dissemination of Intraperitoneal Bacteria by Neutrophil Recruitment. *Immunity*, *47*(2), 374-388.e6. https://doi.org/10.1016/j.immuni.2017.07.018

Stritesky, G. L., Xing, Y., Erickson, J. R., Kalekar, L. A., Wang, X., Mueller, D. L., Jameson, S. C., & Hogquist, K. A. (2013). Murine thymic selection quantified using a unique method to capture deleted T cells. *Proceedings of the National Academy of Sciences*, *110*(12), 4679-4684. https://doi.org/10.1073/pnas.1217532110

Surh, C. D., & Sprent, J. (1994). T-cell apoptosis detected in situ during positive and negative selection in the thymus. *Nature*, *372*(6501), 100-103. https://doi.org/10.1038/372100a0

Tabula, M. C. (2020). A single-cell transcriptomic atlas characterizes ageing tissues in the mouse. *Nature*, *583*(7817), 590-595. https://doi.org/10.1038/s41586-020-2496-1

Tabula, M. C., Overall, C., Logistical, C., Organ, C. A. P., Library, P. A. S., Computational, D. A., Cell, T. A., Writing, G., Supplemental, T. W. G., & Principal, I. (2018). Single-cell transcriptomics of 20 mouse organs creates a Tabula Muris. *Nature*, *562*(7727), 367-372. https://doi.org/10.1038/s41586-018-0590-4

Tacke, R., Hilgendorf, I., Garner, H., Waterborg, C., Park, K., Nowyhed, H., Hanna, R. N., Wu, R., Swirski, F. K., Geissmann, F., & Hedrick, C. C. (2015). The transcription factor NR4A1 is essential for the development of a novel macrophage subset in the thymus. *Scientific Reports*, *5*(1), 10055. https://doi.org/10.1038/srep10055

Tamoutounour, S., Guilliams, M., Sanchis, F. M., Liu, H., Terhorst, D., Malosse, C., Pollet, E., Ardouin, L., Luche, H., Sanchez, C., Dalod, M., Malissen, B., & Henri, S. (2013). Origins and Functional Specialization of Macrophages and of Conventional and Monocyte-Derived Dendritic Cells in Mouse Skin. *Immunity*, *39*(5), 925-938. https://doi.org/10.1016/j.immuni.2013.10.004

Taniuchi, I., Osato, M., Egawa, T., Sunshine, M. J., Bae, S. C., Komori, T., Ito, Y., & Littman, D. R. (2002). Differential requirements for Runx proteins in CD4 repression and epigenetic silencing during T lymphocyte development. *Cell*, *111*(5), 621-633. https://doi.org/10.1016/s0092-8674(02)01111-x

Tsai, T. L., Zhou, T. A., Hsieh, Y. T., Wang, J. C., Cheng, H. K., Huang, C. H., Tsai, P. Y., Fan, H. H., Feng, H. K., Huang, Y. C., Lin, C. C., Lin, C. H., Lin, C. Y., Dzhagalov, I. L., & Hsu, C. L. (2022). Multiomics reveal the central role of pentose phosphate pathway in resident thymic macrophages to cope with efferocytosis-associated stress. *Cell Rep*, *40*(2), 111065. https://doi.org/10.1016/j.celrep.2022.111065

van Furth, R., & Cohn, Z. A. (1968). The origin and kinetics of mononuclear phagocytes. *The Journal of experimental medicine*, *128*(3), 415-435. https://doi.org/10.1084/jem.128.3.415

Vobořil, M., Brabec, T., Dobeš, J., Šplíchalová, I., Březina, J., Čepková, A., Dobešová, M., Aidarova, A., Kubovčiak, J., Tsyklauri, O., Štěpánek, O., Beneš, V., Sedláček, R., Klein, L., Kolář, M., & Filipp, D. (2020). Toll-like receptor signaling in thymic epithelium controls monocyte-derived dendritic cell recruitment and Treg generation. *Nature Communications*, *11*(1), 1-16. https://doi.org/10.1038/s41467-020-16081-3

Wada, H., Masuda, K., Satoh, R., Kakugawa, K., Ikawa, T., Katsura, Y., & Kawamoto, H. (2008). Adult T-cell progenitors retain myeloid potential. *Nature*, *452*(7188), 768-772. https://doi.org/10.1038/nature06839

Wang, H., Breed, E. R., Lee, Y. J., Qian, L. J., Jameson, S. C., & Hogquist, K. A. (2019). Myeloid cells activate iNKT cells to produce IL-4 in the thymic medulla. *Proceedings of the National Academy of Sciences*, *116*(44), 22262-22268. https://doi.org/10.1073/pnas.1910412116

Wang, M., Yang, Y., Cansever, D., Wang, Y., Kantores, C., Messiaen, S., Moison, D., Livera, G., Chakarov, S., Weinberger, T., Stremmel, C., Fijak, M., Klein, B., Pleuger, C., Lian, Z., Ma, W., Liu, Q., Klee, K., Händler, K., . . . Bhushan, S. (2021). Two populations of self-maintaining monocyte-independent macrophages exist in adult epididymis and testis. *Proc Natl Acad Sci U S A*, *118*(1), e2013686117. https://doi.org/10.1073/pnas.2013686117

Witmer-Pack, M. D., Hughes, D. A., Schuler, G., Lawson, L., McWilliam, A., Inaba, K., Steinman, R. M., & Gordon, S. (1993). Identification of macrophages and dendritic cells in the osteopetrotic (op/op) mouse. *Journal of cell science*, *104*(Pt 4), 1021-1029. http://eutils.ncbi.nlm.nih.gov/entrez/eutils/elink.fcgi?dbfrom=pubmed&id=8314887&retmode=ref&cmd=prlinks

1645 Wolf, F. A., Angerer, P., & Theis, F. J. (2018). SCANPY: large-scale single-cell gene
1646 expression data analysis. *Genome Biol*, *19*(1), 15.
1647 https://doi.org/10.1186/s13059-017-1382-0
1648 Wynn, T. A., Chawla, A., & Pollard, J. W. (2013). Macrophage biology in
1649 development, homeostasis and disease. *Nature*, *496*(7446), 445-455.
1650 https://doi.org/10.1038/nature12034
1651 Yahara, Y., Barrientos, T., Tang, Y. J., Puviindran, V., Nadesan, P., Zhang, H.,
1652 Gibson, J. R., Gregory, S. G., Diao, Y., Xiang, Y., Qadri, Y. J., Souma, T.,
1653 Shinohara, M. L., & Alman, B. A. (2020). Erythromyeloid progenitors give rise
1654 to a population of osteoclasts that contribute to bone homeostasis and repair.
1655 *Nature cell biology*, *22*(1), 1-28. https://doi.org/10.1038/s41556-019-0437-8
1656 Yona, S., Kim, K.-W., Wolf, Y., Mildner, A., Varol, D., Breker, M., Strauss-Ayali,
1657 D., Viukov, S., Guilliams, M., Misharin, A., Hume, D. A., Perlman, H.,
1658 Malissen, B., Zelzer, E., & Jung, S. (2013). Fate Mapping Reveals Origins and
1659 Dynamics of Monocytes and Tissue Macrophages under Homeostasis.
1660 *Immunity*, *38*(1), 79-91. https://doi.org/10.1016/j.immuni.2012.12.001
1661 Yu, G., Wang, L.-G., Han, Y., & He, Q.-Y. (2012). clusterProfiler: an R Package for
1662 Comparing Biological Themes Among Gene Clusters. *OMICS: A Journal of*
1663 *Integrative Biology*, *16*(5), 284-287. https://doi.org/10.1089/omi.2011.0118
1664

1665 **Acknowledgments**

1666 We are grateful to the IMMGEN consortium for performing the RNA
1667 sequencing of our samples and providing access to its database. We thank
1668 the following core facilities at National Yang Ming Chiao Tung University:
1669 Instrumentation Resource Center for providing access to its sorting and
1670 imaging facility and the Animal Facility for mouse husbandry. We are very
1671 grateful to Wan-Chun Chang, Bing-Xiu Guo, Chien-Yi Tung, and Kate Hua
1672 from the Genomics Center for Clinical and Biotechnological Applications of
1673 NCFB (NYCU, Taipei) for help with scRNA-Seq. Special thanks go to Dr.
1674 Fang Liao, Academia Sinica, Taipei, for help with cell sorting and for providing
1675 the 24G2 hybridoma, and Chang-Feng Chu for technical assistance. We are
1676 very grateful to Alexandra Norris, Cecilia Tai, and Angelina Shih for the
1677 manual scoring of the in vitro phagocytosis experiments. We are indebted to

Dr. Yu-Wen Su (NHRI, Taiwan) for help with the mice. Some figures were made with BioRender.

This work was supported by the Ministry of Science and Technology, Taiwan (grants # 107-2320-B-010 -016 -MY3, 110-2320-B-A49A-521 - , and 111-2320-B-A49 -031 -MY3 to IL Dzhagalov), the Yen-Tjing Ling Medical Foundation (grant # CI-111-6 to IL Dzhagalov), and the Cancer Progression Research Center (NYCU). The authors declare no competing financial interests.

Supplementary figures and tables

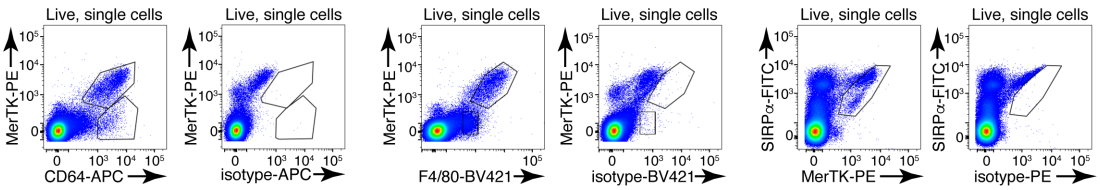

Figure 1 – figure supplement 1: Representative flow cytometry staining of enzymatically digested thymus single-cell suspension for CD64, MerTK, and F4/80 and respective isotype controls. The flow cytometry plots are representative of 5 individual experiments.

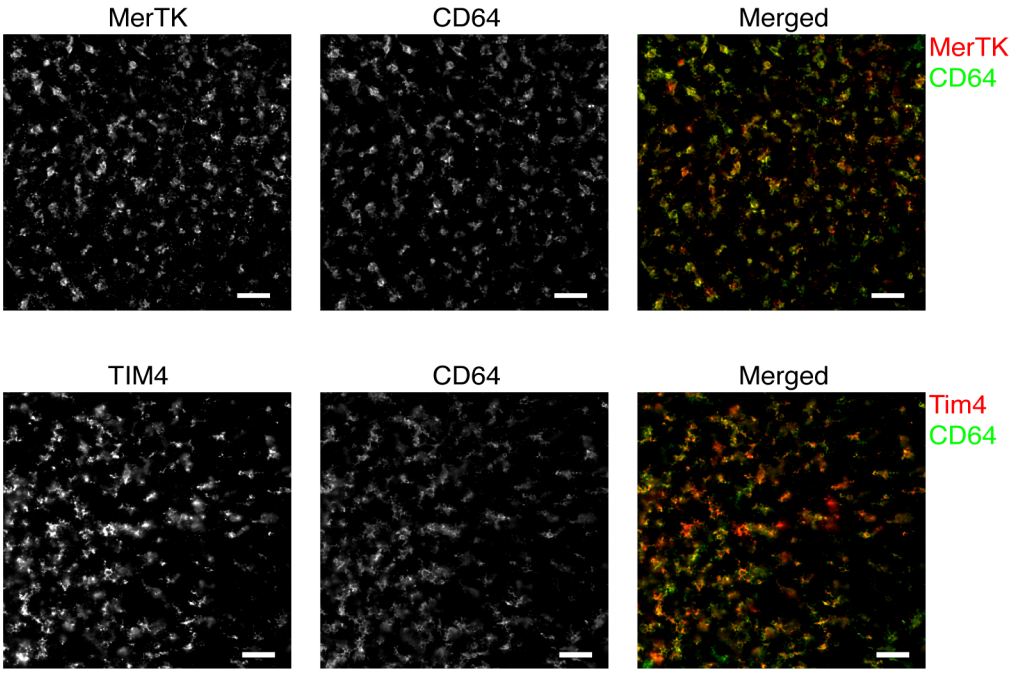

1697

1698 **Figure 1 – figure supplement 2:** Immunofluorescent images of thymic

1699 sections showing co-localization of MerTK and CD64 staining (upper row) and

1700 TIM4 and CD64 staining (lower row) in the thymic cortex. The images are

1701 representative of at least three mice. The scale bar is 50 μm.

1702

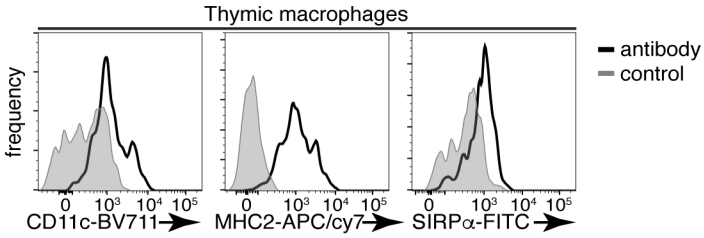

1703

1704 **Figure 1 – figure supplement 3:** Expression of CD11c, MHC2, and SIRPα

1705 on ThyMacs with respective controls. The flow cytometry plots are

1706 representative of 5 individual experiments.

1707

1708 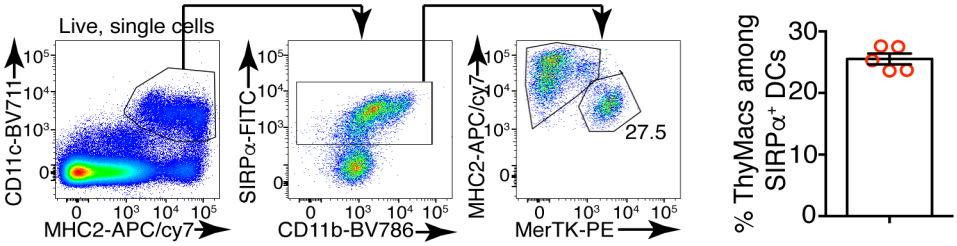

1709 **Figure 1 – figure supplement 4:** Example flow cytometry plots showing
1710 that gating on CD11c$^+$MHC2$^+$ thymus cells, in addition to DCs, also includes
1711 macrophages, especially among SIRPα^+ cells. On the right is a plot of the
1712 frequency of MerTK$^+$ cells among CD11c$^+$MHC2$^+$SIRPα^+ cells. The data are
1713 mean±SEM from 5 individual mice. Each dot is an individual mouse. The
1714 numbers in the flow cytometry plots are the percent of cells in the respective
1715 gate.

1716

1717 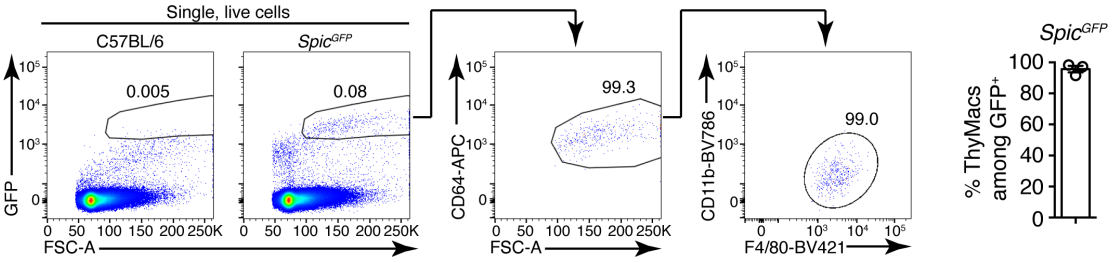

1718 **Figure 2 – figure supplement 1:** Example of the gating strategy to identify
1719 ThyMacs among *Spic*$^{GFP+}$ cells. On the right is a plot showing the mean±SEM
1720 of the frequencies of ThyMacs among *Spic*$^{GFP+}$ cells. Each dot is an individual
1721 mouse. The numbers in the flow cytometry plots are the percent of cells in the
1722 respective gate.

1723

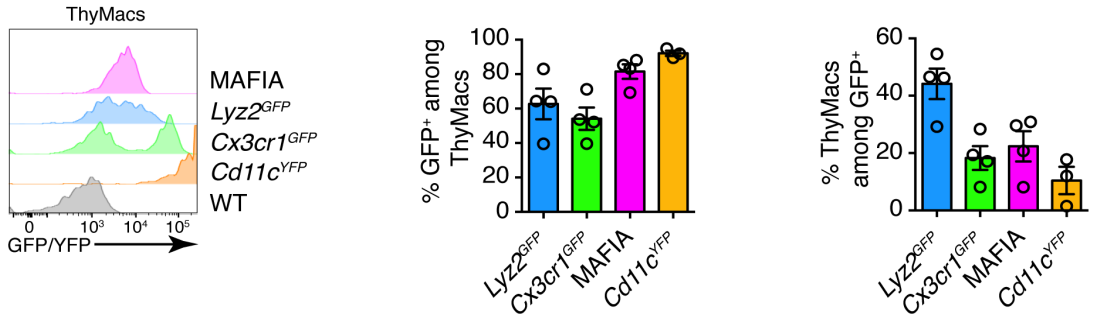

Figure 2 – figure supplement 2: Representative flow cytometry plots of the expression of four reporter alleles in ThyMacs (left), frequencies of GFP/YFP^{+} cells among ThyMacs (middle), and frequencies of ThyMacs among GFP/YFP^{+} cells (right). Data in the graphs represent mean±SEM. Each dot is an individual mouse.

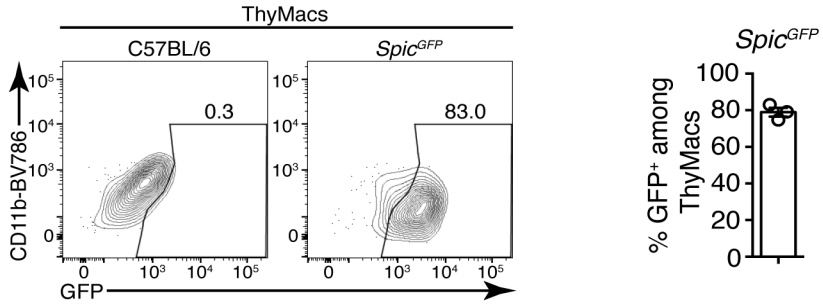

Figure 2 – figure supplement 3: Representative flow cytometry plots of the expression of *Spic*^{GFP} in ThyMacs. To the right is a graph showing the mean±SEM of the frequencies of *Spic*$^{GFP+}$ cells among ThyMacs. Each dot is an individual mouse. The numbers in the flow cytometry plots are the percent of cells in the respective gate.

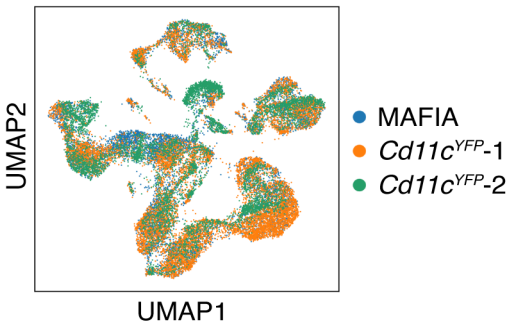

1739

1740 **Figure 4 – figure supplement 1:** UMAP clustering of the scRNA-Seq data

1741 shows that the cells from the three samples (one from GFP$^+$ cells in MAFIA

1742 mice and two from YFP$^+$ cells in *Cd11c*^{YFP} mice) overlap considerably.

1743

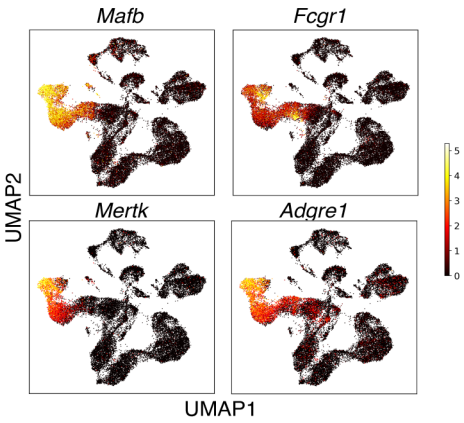

1744

1745 **Figure 4 – figure supplement 2**: The relative expression of prototypical

1746 macrophage genes *Mafb*, *Fcgr1* (CD64), *Mertk*, and *Adgre1* (F4/80) among

1747 thymic cells sorted as *Csf1r*$^{GFP+}$ and *Cd11c*$^{YFP+}$.

1748

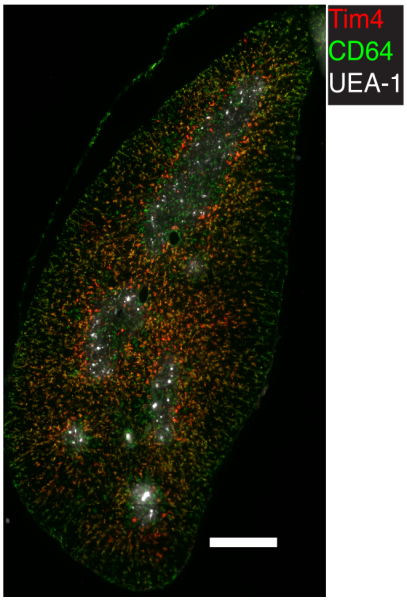

Figure 4 figure supplement 3: Representative immunofluorescent image of WT thymic frozen section stained for TIM4, CD64, and UEA-1 (a marker for medulla). CD64 stains all macrophages, while TIM4 – only a subset that is located in the cortex. The image is representative of 3 mice. The scale bar is 400 μm.

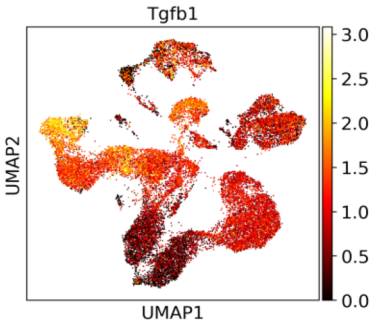

Figure 4 figure supplement 4: The relative expression of *Tgfb1* among thymic cells from the scRNA-Seq data.

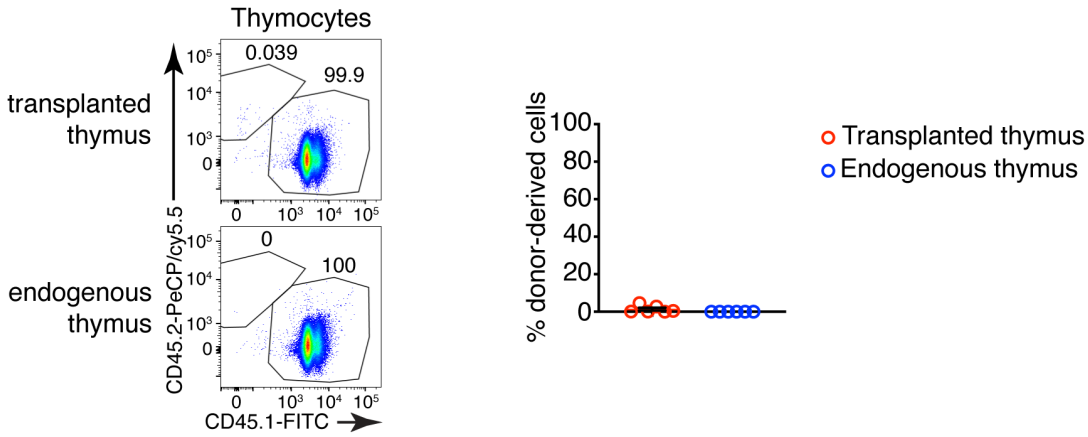

1759

1760 **Figure 5 – figure supplement 1:** Representative flow cytometry plots of
1761 donor (CD45.2⁺) vs. host (CD45.1⁺) derived thymocytes in the transplanted
1762 thymus. The host thymus (endogenous thymus) serves as a negative control.
1763 To the right is a graph showing the mean±SEM of the frequencies of CD45.2⁺
1764 (donor-derived) cells among thymocytes in the transplanted and endogenous
1765 thymuses of the mice. Each dot is an individual mouse. The numbers in the
1766 flow cytometry plots are the percent of cells in the respective
1767 gate.

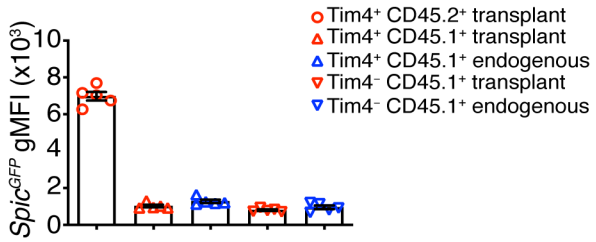

1768

1769 **Figure 5 – figure supplement 2:** Comparison of the geometric mean
1770 fluorescent intensities (gMFI) of *Spic*^{GFP} TIM4⁺ and TIM4⁻ thymic
1771 macrophages of host and donor-origin in the transplanted thymus. The
1772 endogenous thymus serves as background control. Only populations
1773 comprising >5% of thymic macrophages are shown. Each dot is an individual
1774 mouse. The data are presented as mean±SEM.

1775

1776 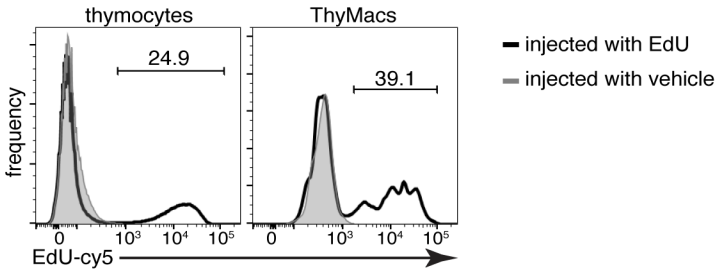

1777 **Figure 6 – figure supplement 1:** Example flow cytometry plots of the EdU
1778 accumulation in thymocytes and thymic macrophages 2 hours after 1 mg EdU
1779 i.p. or vehicle injection. The numbers inside flow plots are the percentage of
1780 EdU^+ cells from mice injected with EdU. Data are representative of three
1781 independent experiments.

1782

1783

Table 1: Expression of differentially up-regulated transcription factors in thymic macrophages

Gene name	ThyMacs	non-ThyMacs
Irf7	3879.32	300.82
Irf8	3528.27	1474.35
Stat1	2403.69	522.04
Dnmt3a	1515.94	647.81
Znxf1	1379.89	635.36
Stat2	1210.35	472.53
Nr1h3	1182.17	147.05
Srebf1	975.09	399.06
Rxra	760.26	298.55
Trps1	746.36	232.48
Runx3	723.14	9.76
Relb	715.53	293.92
Sp100	696.94	324.47
Zbp1	639.19	69.83
Tfec	588.72	74.66
Spic	573.11	34.36
Nfkbie	569.74	226.76
Ncoa4	550.69	249.15
Rest	548.22	269.22
Meis3	530.8	120.91
Bhlhe40	490.59	99.56

Parp12	414.11	126.82
Arid5b	374.03	177.08
Creb5	295.14	47.91
Pparg	276.54	33.24

1784

1785 **Table 2: Expression of differentially up-regulated transcription factors**
1786 **in thymic macrophages.** Transcription factors that were highly expressed in
1787 thymic macrophages (>250) and up-regulated >2-fold in thymic macrophages
1788 compared to non-thymic macrophages were listed alphabetically, and the
1789 geometric means of 4 replicates of thymic macrophages (ThyMacs) and two
1790 replicates of each of the 9 non-thymic macrophage populations (non-
1791 ThyMacs) were recorded. Non-thymic macrophages are: spleen red pulp
1792 macrophages, Kupffer cells, broncho-alveolar lavage macrophages,
1793 peritoneal cavity macrophages, aorta macrophages, heart macrophages,
1794 white adipose tissue macrophages, central nervous system microglia, spinal
1795 cord macrophages.

Table 2: List of the differentially expressed genes among *Timd*4+ thymic macrophages, *Cx3cr1*+ thymic macrophages, and thymic monocytes

***Cx3cr1*+ ThyMacs**		***Timd4*+ ThyMacs**		**ThyMonos**	
Gene name	adjusted p-value	Gene name	adjusted p-value	Gene name	adjusted p-value
Ctsz	0	*Hpgd*	0	*Alox5ap*	0
Cd63	0	*Serpinb6a*	0	*S100a6*	0
Pmepa1	0	*Slc40a1*	0	*Ly6c2*	0
Zmynd15	0	*Cd81*	0	*Ifi27l2a*	0
Olfml3	0	*Vcam1*	0	*Fau*	0
Mmp2	0	*Cfp*	0	*Coro1a*	0
AU020206	1.60E-290	*Spic*	0	*Ccr2*	0
Plxnd1	1.59E-285	*Trf*	0	*Rps27*	0
Cst7	8.68E-279	*Actn1*	0	*Tmsb10*	0
Dnase1l3	2.45E-270	*Maf*	0	*Ifitm2*	7.21E-302
Timp2	2.15E-267	*Pld3*	0	*Fxyd5*	6.36E-299
Lgals3bp	8.69E-263	*Il18*	0	*Rps19*	2.04E-292
Pdgfa	6.87E-255	*Mrc1*	0	*Rpl18*	6.50E-291

Mmp14	2.33E-253	*Crip2*	0	*Rpl9*	1.11E-289
Fam46c	9.99E-235	*Tmem65*	0	*Rps23*	1.28E-289
Chst2	1.19E-226	*Igf1*	0	*Napsa*	8.91E-279
Cp	5.36E-225	*Epb41l3*	0	*Ms4a4c*	8.25E-272
Camk1	7.12E-225	*Timd4*	0	*Plac8*	2.10E-270
B2m	1.09E-222	*Blvrb*	0	*Rpl18a*	9.26E-269
Lhfpl2	4.52E-217	*Clec1b*	0	*S100a4*	4.98E-268
Acp5	5.90E-216	*Cd68*	0	*Cd52*	3.67E-267
Lag3	3.91E-213	*Axl*	0	*Rps14*	1.94E-266
Lyz2	1.28E-209	*Paqr9*	3.32E-307	*Ifitm3*	3.19E-263
H2-M2	1.22E-199	*Sdc3*	3.45E-305	*Rpl34*	2.02E-261
Psap	7.26E-198	*Myo9a*	5.59E-305	*Rps27a*	3.67E-260
Gatm	1.33E-192	*Scp2*	3.79E-302	*Rpl36*	1.54E-259
Cpd	1.50E-192	*Selenop*	2.10E-295	*Rps16*	2.55E-258
C3	2.34E-187	*Lrp1*	2.08E-294	*Rpl24*	1.37E-257
Cxcl16	8.11E-183	*Lap3*	1.45E-290	*Rps9*	6.34E-253
Lgals3	1.57E-182	*Marcks*	2.77E-279	*Gpr141*	1.21E-246
Ube2j1	1.63E-180	*Glul*	3.64E-279	*Rpl27a*	3.06E-243
Plxnc1	9.84E-180	*Hebp1*	3.76E-278	*Rpl17*	8.15E-241
Stab1	4.07E-176	*Ear2*	4.53E-276	*Rps24*	1.46E-240
Cyth1	3.27E-163	*Apoc1*	2.49E-275	*Rps13*	2.34E-236
Spsb1	3.96E-163	*Kcna2*	3.72E-275	*Rpl38*	1.95E-226
Blnk	2.35E-162	*Myo10*	9.05E-269	*H2-DMb1*	1.02E-223
Cx3cr1	9.29E-162	*Atp13a2*	2.95E-267	*Rps18*	5.39E-223
Med10	5.25E-161	*Slc1a3*	6.24E-263	*Rpl19*	3.68E-221
Nek6	5.28E-160	*Slco2b1*	1.11E-258	*Rpl8*	2.01E-219
Ptms	1.05E-159	*mt-Nd2*	3.45E-258	*Rpl7a*	4.17E-217
Anxa5	1.10E-156	*Wwp1*	2.16E-253	*Gm34084*	5.23E-216
Gpnmb	1.21E-154	*Aplp2*	4.22E-248	*Rpl13*	2.08E-215
Itgb5	2.78E-154	*Atp8a1*	5.03E-248	*Rpl11*	2.47E-213
Myo5a	1.11E-146	*P2ry13*	3.17E-247	*Rpl35a*	2.13E-210
Runx3	1.81E-146	*Ccdc148*	4.70E-245	*Rpsa*	1.62E-209
Tmem176a	2.34E-144	*Grn*	1.58E-244	*Rpl6*	5.70E-208
Ctss	4.81E-141	*Bank1*	1.82E-239	*Tpt1*	2.63E-206
Sh3pxd2b	9.38E-141	*Mertk*	2.15E-238	*Rack1*	2.14E-203
Rtcb	4.42E-140	*Nr1h3*	1.13E-235	*Rpl23*	6.14E-199
Fam20c	1.91E-139	*Prnp*	2.93E-235	*Rpl26*	7.48E-198
Il2rg	8.84E-138	*Ninj1*	2.42E-234	*Rps6*	6.64E-197
Lpcat2	8.53E-137	*Fcna*	3.33E-233	*Rps10*	2.06E-195
Kynu	8.49E-136	*Csrp1*	1.16E-230	*Ier5*	1.06E-191
Tnfsf13b	8.77E-136	*Rgl1*	7.18E-229	*Rps3*	8.23E-185
Gpr157	1.18E-135	*Lpl*	4.94E-223	*Rpl27*	8.23E-185
Tgfbr1	7.63E-135	*Fam213b*	1.08E-222	*Rps5*	8.36E-185

H2-K1	1.15E-133	*Tcf7l2*	1.26E-222	*Rps7*	3.96E-182
Basp1	1.23E-133	*AB124611*	4.64E-221	*Rps15a*	6.82E-182
Pla2g7	1.80E-132	*Abcc3*	3.28E-216	*Rps11*	1.97E-180
Fth1	4.19E-131	*Fcgrt*	5.79E-216	*Rps4x*	5.07E-180
Ggh	1.85E-126	*Tgm2*	1.88E-215	*Rplp0*	3.09E-177
Adam19	6.94E-126	*Itgad*	5.35E-214	*Ly6i*	8.17E-176
C3ar1	7.35E-125	*Ptgs1*	2.94E-213	*S100a11*	6.23E-175
Ccl12	3.37E-123	*Laptm4a*	1.01E-212	*Atox1*	1.22E-174
Hvcn1	2.51E-121	*Comt*	1.33E-206	*Pim1*	9.56E-174
Anxa3	8.60E-121	*Creg1*	3.24E-205	*Sh3bgrl3*	3.97E-173
Tgfbi	1.88E-120	*Adgre1*	9.67E-205	*Ciita*	7.35E-173
Ctsd	2.73E-117	*Clec12a*	6.33E-204	*Eef1a1*	6.09E-172
Itm2c	5.19E-116	*Tspan4*	7.80E-203	*Rps3a1*	9.09E-168
Tmem119	5.62E-116	*Txn1*	9.13E-203	*Gm2a*	6.07E-165
Rap2a	1.03E-114	*Ctsb*	9.52E-201	*Ptprc*	2.05E-163
Ctsl	4.00E-114	*Mrap*	5.65E-197	*Rpl37*	1.51E-161
Itga6	1.83E-113	*Slc16a9*	5.99E-197	*Rps25*	3.03E-160
B4galnt1	2.45E-113	*Abcg3*	3.83E-196	*H3f3a*	5.92E-159
Fam3c	1.64E-112	*Pla2g15*	4.22E-196	*Btg2*	1.14E-158
Tmem173	1.54E-111	*C1qc*	6.17E-192	*Rpl15*	1.42E-158
Ski	3.59E-111	*Agpat3*	1.68E-191	*Cnn2*	1.09E-156
Anpep	5.85E-111	*Hs6st1*	1.95E-191	*Cdkn1a*	2.57E-156
Gng2	2.37E-110	*Dmpk*	2.15E-191	*Slfn1*	4.83E-155
Nceh1	2.88E-110	*Cd38*	1.79E-190	*Sem1*	4.08E-154
H2-Q7	4.94E-108	*Tmem26*	2.02E-189	*Lsp1*	1.34E-152
Rtn1	1.28E-106	*Slc11a1*	1.05E-188	*Rpl37a*	1.78E-152
Sorl1	1.31E-103	*Cd300a*	1.41E-187	*Rpl22*	3.64E-152
Glipr1	1.22E-102	*Slc7a7*	3.28E-187	*Sirpb1c*	4.81E-152
Gsn	2.00E-102	*Cyb5a*	6.94E-187	*Traf1*	6.97E-152
Afdn	4.54E-102	*Sipa1l1*	7.41E-187	*Emb*	4.22E-151
Ak2	1.11E-101	*Il18bp*	1.48E-186	*Rpl30*	1.32E-147
Ntpcr	2.21E-98	*Cd86*	2.52E-183	*Rps15*	1.14E-146
Scarb2	3.16E-97	*Vamp5*	3.05E-183	*H2-Ab1*	2.84E-145
Creb5	5.41E-97	*Jup*	6.69E-182	*Il1b*	3.05E-145
Gsto1	5.56E-97	*Blvra*	1.30E-178	*Rps28*	4.52E-145
Ncf1	4.26E-96	*Mgst1*	6.48E-178	*Jarid2*	1.82E-143
Ppfia4	4.97E-96	*Tbxas1*	1.47E-177	*Rps26*	1.53E-142
Chchd10	7.77E-96	*Hpgds*	2.04E-177	*Rpl32*	4.21E-142
Gna12	1.23E-95	*Tgfbr2*	2.70E-176	*Pld4*	9.07E-142
Mvb12b	1.80E-95	*Clec4n*	3.52E-175	*Cbfa2t3*	1.54E-141
Rasal3	1.45E-94	*Ms4a7*	5.30E-175	*Rps21*	4.04E-141
Scoc	6.86E-94	*Sirpa*	3.35E-171	*Fgr*	4.04E-141
Cfb	6.00E-93	*Fyn*	2.84E-168	*Rps8*	1.11E-139

Lmna	1.04E-92	*Cadm1*	2.20E-167	*Cd74*	5.34E-138

1796

1797 **Table 2: List of the differentially expressed genes among *Timd4*$^{+}$**

1798 **thymic macrophages, *Cx3cr1*$^{+}$ thymic macrophages, and thymic**

1799 **monocytes.** The top 100 differentially expressed genes among the three

1800 clusters are listed by their negative $\log_{10}$ transformed p-value.

1801

1802
1803